Endothelial caveolin-1 regulates cerebral thrombo-inflammation in acute ischemia/reperfusion injury

Xiaohao Zhang,[a,b,c,1] Pengyu Gong,[d,1] Ying Zhao,[a,1] Ting Wan,[a] Kang Yuan,[a] Yunyun Xiong,[e,f,g] Min Wu,[h] Mingming Zha,[a] Yunzi Li,[a] Teng Jiang,[b] Xinfeng Liu,[a] Ruidong Ye,[a] Yi Xie,[a]* and Gelin Xu[a]*

[a]Department of Neurology, Affiliated Jinling Hospital, Medical School of Nanjing University, Nanjing, Jiangsu 210000, China
[b]Department of Neurology, Nanjing First Hospital, Nanjing Medical University, Nanjing, Jiangsu 210000, China
[c]Department of Neurology, Jiangsu Provincial Second Chinese Medicine Hospital, Second Affiliated Hospital of Nanjing University of Chinese Medicine, Nanjing, Jiangsu 210000, China
[d]Department of Neurology, Affiliated Hospital of Nantong University, Nantong 226000, China
[e]Department of Neurology, Beijing Tiantan Hospital, Capital Medical University, Beijing 100070, China
[f]China National Clinical Research Center for Neurological Diseases, Beijing 100070, China
[g]Chinese Institute for Brain Research, Beijing 100070, China
[h]Department of Neurology, Jinling Hospital, Nanjing Medical University, Nanjing, Jiangsu 210000, China

eBioMedicine 2022;84: 104275
Published online xxx
https://doi.org/10.1016/j.ebiom.2022.104275

Summary

Background Thrombo-inflammation is an important checkpoint that orchestrates infarct development in ischemic stroke. However, the underlying mechanism remains largely unknown. Here, we explored the role of endothelial Caveolin-1 (Cav-1) in cerebral thrombo-inflammation.

Methods The correlation between serum Cav-1 level and clinical outcome was analyzed in acute ischemic stroke patients with successful recanalization. Genetic manipulations by endothelial-specific adeno-associated virus (AAV) and siRNA were applied to investigate the effects of Cav-1 in thrombo-inflammation in a transient middle cerebral artery occlusion (tMCAO) model. Thrombo-inflammation was analyzed by microthrombosis formation, myeloid cell infiltration, and endothelial expression of adhesion molecules as well as inflammatory factors.

Findings Reduced circulating Cav-1, with the potential to predict microembolic signals, was more frequently detected in recanalized stroke patients without early neurological improvement. At 24 h after tMCAO, serum Cav-1 was consistently reduced in mice. Endothelial Cav-1 was decreased in the peri-infarct region. *Cav-1*$^{-/-}$ endothelium, with prominent barrier disruption, displayed extensive microthrombosis, accompanied by increased myeloid cell inflammatory infiltration after tMCAO. Specific enhanced expression of endothelial Cav-1 by AAV-*Tie1-Cav-1* remarkably reduced infarct volume, attenuated vascular hyper-permeability and alleviated thrombo-inflammation in both wild-type and *Cav-1*$^{-/-}$ tMCAO mice. Transcriptome analysis after tMCAO further designated *Rxrg* as the most significantly changed molecule resulting from the knockdown of Cav-1. Supplementation of RXR-γ siRNA reversed AAV-*Tie1-Cav-1*-induced amelioration of thrombo-inflammation without affecting endothelial tight junction.

Interpretation Endothelial Cav-1/RXR-γ may regulate infarct volume and neurological impairment, possibly through selectively controlling thrombo-inflammation coupling, in cerebral ischemia/reperfusion.

Funding This work was supported by National Natural Science Foundation of China.

Keywords: Caveolin-1; Inflammation; Ischemic stroke; Microthrombosis; Vascular endothelium

Introduction

Stroke is a worldwide leading cause of death and permanent disability, among which ischemic stroke accounts for 80%.[1] Despite a high recanalization rate of approximately 75–80% achieved by endovascular thrombectomy (EVT), infarcts often continue to increase in size, leading to progressive neurological deterioration and

*Corresponding authors at: Department of Neurology, Jinling Hospital, Medical School of Nanjing University, No. 305 East Zhongshan Rd, Nanjing, Jiangsu 210000, China.
E-mail addresses: xy_307@126.com (Y. Xie), gelinxu@nju.edu.cn (G. Xu).

[1] X. Zhang, P. Gong, and Y. Zhao contributed equally to this work. Y. Xie and G. Xu are co-senior authors.

Research in context

Evidence before this study

The concerted action of the thrombotic and inflammatory pathway plays a pathogenic role in promoting infarct progression in cerebral ischemic stroke. Targeting platelet-leukocyte interaction has been proven effective. Endothelial dysfunction is the early prerequisite of thrombo-inflammatory events in cerebral I/R injury. However, except for the published role of endothelial vWF, little is known about the mechanism underlying the involvement of inflamed endothelium in microthrombosis. Previous studies have suggested caveolin-1 (Cav-1) is required in maintaining vascular homeostasis.

Added value of this study

We find an important clinical association of circulating Cav-1 level with early neurological improvement in recanalized stroke patients. Mechanistically, endothelial Cav-1, independent of the caveolae organelle, is responsible to regulate thrombo-inflammatory activity in the peri-infarct area. Furthermore, we designate RXR-γ as a downstream effector of Cav-1. Regulation of microvascular Cav-1/RXR-γ signaling selectively manipulates microthrombus formation and vascular inflammation without affecting microvascular permeability.

Implications of all the available evidence

In cerebral I/R injury, specific regulation of endothelial Cav-1/RXR-γ controls the coupling of thrombosis and inflammation, which could further mediate tissue damage. Our study suggests that endothelial Cav-1/RXR-γ signaling might be a specific checkpoint under ischemic thrombo-inflammatory conditions.

unfavorable outcomes in a considerable proportion of patients.[2–4] Microvascular events, which depend on the concerted action of immune cells and platelets, are most likely to be responsible for the ongoing infarct development.[5–7] At the sites of vascular ischemic injury, the binding of platelets on endothelial von Willebrand factor (vWF) triggers initial deposition and activation of platelets, followed by coagulation system activation.[8–10] The activation of coagulation throughout the microcirculation is always accompanied by an intense inflammatory response in ischemia/reperfusion (I/R) injury.[11,12] Upregulation of endothelial cell adhesion molecules, such as vascular cell adhesion molecule-1 (VCAM-1) and intercellular cell adhesion molecule-1 (ICAM-1), in the microvasculature, associated with platelet-leukocyte adhesion, promotes the recruitment of immune cells and guide inflammation in response to ischemia.[13–15] As thrombosis promotes inflammation, the immune cells, in turn, could stimulate thrombus formation.[16] Several recent findings demonstrate that concurrent targeting of both thrombotic and inflammatory processes could afford protections for acute ischemic stroke,[17,18] suggesting that thrombo-inflammation may be therapeutically targetable.

The endothelium is a critical regulator of thrombo-inflammation.[19] Quiescent endothelial cells in the microvasculature have natural properties of anticoagulant and anti-inflammation to maintain vascular health.[11] However, following the abrupt arrest of cerebral blood flow, endothelial cells bear the major brunt of injuries, such as the sudden change in shear stress and hypoxia-associated toxicity. Dysfunctional endothelial cells could release prothrombotic and proinflammatory factors, which may promote the process of thrombo-inflammation in microcirculation.[20,21] Therefore, a better understanding of the mechanism underlying the perturbed function of endothelial cells after I/R injury may result in novel therapeutics for thrombo-inflammation and subsequent brain damage.

Caveolin-1 (Cav-1) is highly expressed in endothelial cells and is vital for caveolae biogenesis in the endothelium, orchestrating signal transduction and endothelial vesicular trafficking.[22] Through regulating the degradation of matrix metalloproteinases, extracellular matrix, and tight junction (TJ) proteins, Cav-1 could determine endothelial barrier integrity following stroke.[23–26] In patients with ischemic stroke, a reduced level of Cav-1 was associated with cerebral microbleeds[27] and symptomatic bleeding[28] after thrombolytic therapy, suggesting an important role of Cav-1 in disrupted endothelial permeability after stroke. This Cav-1-dependent endothelial instability may associate with vascular inflammation.[29] Notably, except for mediating inflammation, Cav-1 could be phosphorylated at Tyr14 in response to several stimuli and linked to platelet cytoskeleton participating in focal adhesions dynamics.[30] However, to date, whether endothelial Cav-1 could participate in thrombo-inflammation after acute ischemic stroke has remained elusive.

To address this important issue, we evaluated the involvement of endothelial Cav-1 in thrombo-inflammation in both human samples and a mouse model of transient middle cerebral artery occlusion (tMCAO). It was remarkable to note that human serum Cav-1 level, with the potential to predict microembolic signals (MES), was associated with early neurological improvement in ischemic stroke patients treated by EVT. In tMCAO mice, endothelial Cav-1, not caveolae, was an important regulator of thrombo-inflammation. Furthermore, RXR-γ, which could not ameliorate endothelial TJ loss, was found required in Cav-1-dependent attenuation of thrombo-inflammation.

Methods

Ethics statement

All experimental protocols were approved by the Jinling Hospital Animal Care Committee and were conducted

following the National Institutes of Health Guide for the Care and Use of Laboratory Animals (NIH Publications No. 8023, revised 2011). The participants or legal representatives who acknowledged the use of blood samples signed an informed consent form before being included in the study. Ethics approval was granted by the ethics committee of Jinling Hospital and Nanjing First Hospital (2016NZGKJ-022; 2019-695).

Antibodies

Antibodies against Collagen IV (Cat# ab6586, RRID: AB_305584), fibrinogen (Cat# ab58207, RRID: AB_941597), serum albumin (Cat# ab19194, RRID: AB_777886), ICAM-1 (Cat# ab179707, RRID: AB_2814769), VCAM-1 (Cat# ab134047, RRID: AB_2721053), TNF alpha (Cat# ab66579, RRID: AB_1310759), PAI-1 (Cat# ab66705, RRID: AB_1310540), CD11b (Cat# ab133357, RRID: AB_2650514), GFAP (Cat# ab53554, RRID: AB_880202), NeuN (Cat# ab104224, RRID: AB_10711040) and vWF (Cat# ab174290, RRID: AB_2802090) were purchased from Abcam, UK; antibody against CD31 (Cat# 550274, RRID: AB_393571) was purchased from BD Biosciences, USA; antibodies against β-actin (Cat# 8457, RRID: AB_10950489), Cav-1 (Cat# 3267, RRID: AB_2275453) and GFP (Cat# 2955, RRID: AB_1196614; Cat# 2956, RRID: AB_1196615) were purchased from Cell Signaling Technology, USA; antibody against Occludin (R1510-33) was purchased from Huabio, China; antibodies against Ly6G (Cat# 14-5931-82, RRID: AB_467730) and, Occludin (Cat# 711500, RRID: AB_88065) and ZO-1 (Cat# 617300, RRID: AB_138452) were purchased from Invitrogen, USA; antibodies against RXR-γ (Cat# sc-514134, RRID: AB_2737293), Iba-1 (Cat# sc-32725, RRID: AB_667733), ZO-1 (Cat# sc-33725, RRID: AB_628459), IL-1β (Cat# sc-12742, RRID: AB_627791), Ly6G (Cat# sc-53515, RRID: AB_783639), α-SMA (Cat# sc-53142, RRID: AB_2273670) and PDGFRβ (Cat# sc-374573, RRID: AB_10990921) were purchased from Santa Cruz Biotechnology, USA; antibodies against CC1 (Cat# OP80, RRID: AB_2057371) was purchased from Millipore, USA; antibodies against thrombocyte (Cat# LS-C348178) was purchased from LifeSpan Biosciences, USA; antibody against mouse IgG (Cat# 115-067-003, RRID: AB_2338586) was purchased from Jackson, USA. All antibodies were used at a dilution of 1:50−1:1000 for immunofluorescence, 1:500−1:1000 for immunoblotting analysis unless otherwise specified. Secondary antibodies were donkey-anti-mouse (conjugated with Alexa 488, Cat# 715-545-150, RRID: AB_2340846; conjugated with Alexa 594, Cat# 715-585-150, RRID: AB_2340854, Jackson, USA; 1:400), or anti-rabbit (conjugated with Alexa 488, Cat# 711-545-152, RRID: AB_2313584; conjugated with Alexa 594, Cat# 711-585-152, RRID: AB_2340621; conjugated with Alexa 647, Cat# 711-605-152, RRID: AB_2492288, Jackson, USA; 1:400), or anti-rat (conjugated with Alexa 488, Cat# 112-545-003, RRID: AB_2338351; conjugated with Alexa 594, Cat# 112-585-003, RRID: AB_2338372, Jackson, USA; 1:400), goat anti mouse (Cat# 7076, RRID: AB_330924, Cell Signaling Technology, USA; 1:5000) or rabbit (Cat# 7074, RRID: AB_2099233, Cell Signaling Technology, USA; 1:5000) or rat (Cat# 7077, RRID: AB_10694715, Cell Signaling Technology, USA; 1:5000) IgG HRP. Purified anti-mouse CD16/32 Antibody (Cat# 101302, RRID: AB_312801, Biolegend, USA), Alexa Fluor® 647 anti-mouse Ly-6G Antibody (Cat# 127609, RRID: AB_1134162, Biolegend, USA), APC/Cyanine7 anti-mouse Ly-6C Antibody (Cat# 128026, RRID: AB_10640120, Biolegend, USA), PE anti-mouse CD45 Antibody (Cat# 103105, RRID: AB_312970, Biolegend, USA), and PE/Cyanine7 anti-mouse/human CD11b Antibody (Cat# 101215, RRID: AB_312798, Biolegend, USA) were used for flow cytometry.

Animals

Male adult C57BL/6J mice weighing 23−25 g were purchased from GemPharmatech Co., Ltd (Nanjing, Jiangsu, China). *Cav-1*$^{-/-}$ mice (Cav-1$^{tm1Mls/J}$, C57BL/6 background, 007083) were purchased from the Jackson Laboratory (Bar Harbor, Maine, USA). Animals were housed in individual cages with a 12 h light/dark cycle at 25 °C and relative humidity of 65% and given free access to food and water. All animal experiments used randomization to treatment groups and blinded assessment. The sample size was decided considering the minimal use of animals. All efforts were made to minimize the number of animals killed and their suffering in the study.

tMCAO surgery

The cerebral I/R model was induced by a 90-min tMCAO according to the previous methods.[31] Briefly, mice were anesthetized with 2−3% isoflurane (RWD Life Science, China). The right common carotid artery, external carotid artery (ECA), and internal carotid artery (ICA) were carefully dissected. The right ECA was ligated and a silicon-coated monofilament (diameter 0.23 ± 0.02 mm) was inserted through the ECA and advanced into the ICA to occlude the origin of the middle cerebral artery (MCA). The cerebral blood flow (CBF) was monitored with the Laser Doppler flowmetry (Perimed PF5000). A reduction of > 70% of baseline CBF was defined as successful occlusion. The filament was withdrawn to induce reperfusion 90 min after occlusion. During the operation, the mice's body temperature was maintained at 37 ± 0.5 °C by a heating pad during surgery. For sham operations, all procedures were performed except that the monofilament was not

inserted. Mice were all sacrificed 24 h after ischemic stroke.

Infarct volume evaluation

For TTC staining, mice brains were cut into consecutive coronal slices of 1 mm thickness. The brain sections were incubated with 2% TTC (Sigma-Aldrich) for 15 min at 37 °C, and further fixed in 4% paraformaldehyde (PFA). The infarct volume was also identified by high signals acquired from T2-weighted images and further confirmed by diffusion-weighted imaging (DWI). Mice were anesthetized with isoflurane and underwent MRI examination using a 7.0 T MRI (Bruker PharmaScan, Germany) 24 h post-stroke. Heart and respiration rates were continuously monitored during the examination. The following parameters of T2-weighted images were used: matrix = 256 × 256, field of view = 20 mm × 20 mm, repetition time = 2800 ms, echo time = 50 ms, and slice thickness = 0.5 mm (18 slices per animal). The following parameters of DWI were used: matrix = 256 × 256, field of view = 20 mm × 20 mm, repetition time = 5000 ms, echo time = 22 ms, and slice thickness = 0.5 mm (18 slices per animal).

The relative infarct volume in both TTC staining and T2-weighted images scan was calculated according to a previous study.[32] Briefly, non-infarcted volume in the lesioned hemisphere and the volume of the contralateral hemisphere were summed and multiplied by the thickness (0.5 mm for MRI and 1.0 mm for TTC staining). Therefore, the relative infarct volume was calculated as (contralateral hemisphere volume − non-infarcted volume in the lesioned hemisphere)/(2 × contralateral hemisphere volume) × 100%.

Neurological function assessment

After 24 h of the surgery, the neurological function of experimental mice was assessed by a modified neurologic severity score (mNSS).[33] The mNSS included a motor functions test, sensory functions test, balancing functions test, and reflex functions and abnormal movements. The total score of mNSS ranged from 0 to 18, and the higher score represents more severe deficits. The neurological function assessment was performed by 2 independent investigators who were blinded to the animal groupings. In case of disagreement, the sub-item and total score were ascertained by consensus.

Cell isolation and culture conditions

As previously published,[34] cerebral blood vessel segments were isolated by layered centrifugation from 6−8-week-old wild-type mice. The pallet of fragments was digested in collagenase/dispase (1 mg/ml, Roche) and DNase I (10 μg/ml, Roche) at 37 °C. The dissociated BMECs were seeded onto coated plates in DMEM/F12 media with 20% FBS, 1% PS, 1% endothelial cell growth supplement (SclenCell), 1% l-glutamine, 1% heparin, and 2 ng ml^{-1} bFGF (Biolegend). Mixed glial cultures from 1- to 2-day-old pups were grown for 7 days. Cells were maintained in DMEM/F12 medium with 10% FBS and 1% PS. Primary mouse oligodendrocyte precursor cells (OPCs) were isolated as reported.[35] The rest of the adherent cells were collected for astrocyte culture. For OPCs proliferation, cells were cultured in DMEM/F12 with 20 ng/ml PDGF (Biolegend), 20 ng/ml bFGF (Biolegend), 20ng/ml ITSS (Roche) and 1% BSA (Gibco). For OPCs differentiation, the medium was switched to DMEM/F12 containing 40 ng/ml T3 (Sigma), 20 ng/ml CNTF (Protein specialists), 1 × N-acetyl-L-cysteine (NAC, Sigma), 20 ng/ml ITSS and 1% BSA. Microglia were shaken off and seeded onto plates after the mixed glial culture was maintained for 14 days. The neurons were isolated and cultured from female mice at 16−18 days of pregnancy.[36] The neuron maintenance medium was neurobasal (Gibco) containing 2% B27 (Gibco), and 1% GlutaMAX (Gibco).

Immunofluorescence

Anesthetized mice were successively perfused intracardially with 0.9% sodium chloride and 4% PFA. The brains were fixed in 4% PFA for 4−6 h and then dehydrated in a gradient sucrose solution (10%, 20%, and 30%) at 4 °C. After being embedded in an optimal cutting temperature compound (Sakura Finetek, USA), the mouse brains were sliced into 18 μm sections. For staining, sections were blocked with 0.3% Triton, 3% goat serum, and 1% bovine serum albumin for 60 min and then incubated with the indicated primary antibodies at 4 °C overnight. The primary antibodies were used at a dilution of 1:50−1:1000 unless otherwise specified. On the second day, the sections were incubated with a secondary antibody and DAPI (Sigma-Aldrich, USA). Secondary antibodies were donkey-anti-mouse, anti-rabbit, or anti-rat conjugated with either Alexa 488 or Alexa 594, or Alexa 647 (Jackson, USA; 1:400). Images were captured with LSM800 confocal microscope (Zeiss, Germany) and Olympus BX51 microscope (Olympus, Japan).

Hematoxylin-eosin (HE) staining

Frozen sections were stained with hematoxylin for 4 min and eosin for 1 min. After gradient washed with ethanol and xylene, the slides were covered lipped with permount, and assessed by a light microscope. The number of occluded microvessels was calculated in the per-infarct area (including cortex, corpus callosum, and striatum). Data were presented as the number of occluded microvessels per mm^2 area.

Microvascular perfusion and permeability assessment

To assess the microvascular perfusion, 5.0 mg per mouse of fluorescein isothiocyanate (FITC)-dextran

(2000 kDa, Sigma, St. Louis, MO, USA) was dissolved in 200 μl PBS and injected through the tail vein. To illustrate the microvascular permeability, another FITC-dextran with a small molecular weight (3 kDa, Sigma, St. Louis, MO, USA) was used. The brains were rapidly removed and placed in 4% PFA for 4–6 h. The coronal sections of 50-μm thick from each mouse were used for immunofluorescence. To label the microvascular endothelium, sections were incubated with anti-CD31, followed by incubation with the secondary antibody. Images were acquired by a BX51 microscope (Olympus, Japan). Data were presented as the numbers of FITC pixels divided by the numbers of CD31 pixels per mm^2.

Flow cytometry analysis

The infarct hemisphere was extracted and further processed as previously described.[18] Cells were washed and incubated with the dead cell marker (Fixable Viability Dye eFluor™ 506, Invitrogen, 65-0866) on ice. Cell suspensions were then incubated with flow cytometry antibodies. Sample analysis was performed using BD Aria II (Becton Dickinson). Data were analyzed using FlowJo software.

Transmission electron microscopy (TEM)

The peri-infarct tissue (1 × 1 × 1 mm) was fixed in 2.5% glutaraldehyde and then processed as previously described.[31] The sections were scanned using H7500 Transmission Electron Microscope (Hitachi, Japan) and were calculated using Image J software (NIH, USA).

RNA-sequencing (RNA-seq) analysis and real-time PCR

Total RNA of peri-infarct tissue from the tMCAO model and sham-operated mice of both wild-type and *Cav-1*$^{-/-}$ mice (n = 4/group) was extracted using TRIzol Reagent (Invitrogen, USA) according to the manufacturer's protocol. The quantity and integrity of RNA yield were evaluated using the K5500 (Beijing Kaiao, China) and Agilent 2200 TapeStation (Agilent Technologies, USA). Briefly, the mRNA was enriched by oligo dT according to instructions of NEB Next® Poly(A) mRNA Magnetic Isolation Module (NEB, USA). The RNA fragments were subjected to the first strand and second strand cDNA synthesis followed by adaptor ligation and enrichment with a low-cycle according to the manufacturer's protocol (NEBNext® Ultra™ RNA Library Prep Kit for Illumina®, USA). The purified library products were assessed by the Agilent 2200 TapeStation and Qubit (Thermo Fisher Scientific, USA). The libraries were sequenced by Illumina (Illumina, USA) with paired-end 150 bp at Ribobio Co. Ltd (Guangzhou, China). An adjusted P value of < 0.05 was set to detect differentially expressed genes with at least a two-fold change of expression. Quantitative real-time PCR was performed on a Stratagene Mx3000P real-time PCR system (Agilent Technologies, USA) using SYBR Premix ExTaq kit (ComWin Biotech, China) for detection. The condition for amplification were pre-denaturation at 95 °C for 30 s, 35 cycles of denaturation at 95 °C for 5 s, and annealing/extension at 60 °C for 20 s.[37] The level of glyceraldehyde-3-phosphate dehydrogenase (GAPDH) of each sample was used for normalization. The primer pairs are listed in Supplemental Table 1.

Immunoblotting

The peri-infarct tissue from wild-type and *Cav-1*$^{-/-}$ mice was extracted 24 h after tMCAO surgery. The brain peri-infarct region was determined according to the previous study.[18,38] Briefly, a longitudinal cut (from dorsal to ventral) with a width of approximately 2 mm from the midline was made in the right infarct hemisphere and the brain tissue was abandoned. Then, another longitudinal cut was performed to separate the peri-infarct region from the white ischemic core. The homogenate of the peri-infarct brain tissue was centrifugated at 1200 rpm for 5 min at 4 °C. The pallet was then resuspended in 15% dextran solution (mol wt 60,000–76,000, Sigma-Aldrich) and centrifugated twice at 2000 rpm for 10 min to isolate microvessels. The supernatant and upper myelin debris were discarded, while the microvascular segment at the bottom was resuspended in RIPA lysis buffer (Cell Signaling Technology, USA) with 1% PMSF. The concentration of protein was quantified by BCA Protein Assay Kit (Beyotime, PR China). An equal amount of protein samples was loaded, separated by SDS-PAGE, and incubated with primary antibodies overnight at 4 °C at a dilution of 1:500–1:2000 unless otherwise specified. After incubation with secondary antibodies on the other day, the protein signals were detected by Immobilon Western Chemiluminescent HRP substrate (Millipore, USA), and were quantified by Image J software (NIH, USA). The expression of β-actin served as the internal control.

Small interfering RNA (siRNA) transfection and adeno-associated virus (AAV) injection

Cav-1 siRNA, RXR-γ siRNA, and negative control (N.C.) siRNA were synthesized by Ribo Bio, Co., Ltd (Guangdong, China). A total of 100 μg siRNA was injected into mice via tail vein every 3 days for 5 injections (20 μg per injection). Endothelial-specific adeno-associated virus (AAV) was conducted by GeneChem co., Ltd (Shanghai, China). The AAV vector with *Tie1* promoter (AAV-*Tie1*-MCS-EGFP-3Flag-SV40 PolyA) was employed to induce the expression of Cav1 in the endothelium. Briefly, the mouse *Cav1* (NM_007616) was constructed on the AAV vector to generate the recombinant plasmid. AAV-293 cells were transfected with the recombinant plasmid. Three days after transfection, the recombinant AAV9 virus was assembled in the packaged cells. Then the

AAV-293 cells were lysed to collect the virus supernatant, followed by CsCl density gradient centrifugation and ultrafiltration. Finally, viral titers were verified using quantitative PCR. The obtained *Cav1*-overexpressing AAV was named AAV-*Tie1-Cav-1*. The viral vectors were stereotaxically injected into the lateral ventricles (0.5 mm anterior−posterior, 1.0 mm medial-lateral, −2.0 mm dorsal-ventral relative to bregma) 3 weeks before tMCAO surgery. All mice received 3 μl of either AAV-*Tie1*-C (1.13 × E13 v.g/ml) or AAV-*Tie1-Cav-1* (1.95 × E13 v.g/ ml).

Study patients and baseline data collection

The ischemic stroke receiving EVT were prospectively enrolled in Jinling Hospital and Nanjing First Hospital during September 2019 and July 2021. The inclusion criteria were as follows: (1) treated with successful EVT [modified Thrombolysis in Cerebral Infarction score of 2b or 3;[4,39] (2) aged > 18 years; (3) had a pre-stroke modified Rankin Scale score ≤ 2; (4) had occlusion of ICA or MCA confirmed by computed tomographic angiography, magnetic resonance angiography, or digital subtracted angiography. Patients with a malignant tumor, autoimmune disease, hematological disease, and active or chronic inflammatory diseases were excluded from this study. Demographic characteristics, medical history, clinical and laboratory data, stroke characteristics, and procedural characteristics were collected after admission using a standardized case report form.

Measurement of serum Cav-1

In ischemic stroke patients, blood samples were obtained after EVT, usually within 24 h of stroke onset. In tMCAO mice, blood samples were obtained at 24 h after the surgery. The blood specimens were centrifuged at 1200 rpm for 10 min and the isolated serum frozen was at −80 °C for further analysis. Enzyme-linked immunosorbent assay (ELISA) was conducted to measure the serum Cav-1 levels (Human Cav-1 ELISA Kit, Cat# EK1494, Sabbiotech, USA; Mouse Cav-1 ELISA Kit, Cat# LS-F35458-1, LSBio, USA).

MES detection

The bilateral main trunk of the middle cerebral artery segments was insonated using a 2-MHz pulsed-wave probe, fixed to a probe-holder with a sample volume of 5 mm. The range of insonation depth was 55−60 mm. According to the international consensus,[40] MES was identified if a signal met these criteria: (1) duration < 300 ms, (2) amplitude > 3 dB concerning underlying flow signal, (3) unidirectionality, and (4) typical sound (snap or chirp). The measurement of MES was performed by an experienced observer who was blinded to the clinical data.

Clinical outcome assessment

The evaluation of neurological deficits was performed using the NIHSS at admission and 24 h after EVT. In our study, we used early neurological improvement (ENI) to assess the development of neurological deficits in the acute phase of stroke. ENI was defined as a reduction of total NIHSS score within 24 h after EVT ≥ 6 points compared with the initial NIHSS.[41]

Statistical analysis

Continuous variables were presented as mean ± SD or median (interquartile range), and categorical variables were summarized as counts and percentages. Categorical variables were compared by chi-square test or Fisher exact test and continuous variables by unpaired t-test, Mann-Whitney U test, or one-way ANOVA followed by Tukey post hoc test. We further performed the spline regression model to explore the shape of the association between serum Cav-1 and clinical outcomes, fitting a restricted cubic spline function with 3 knots (at 5th, 50th, and 95th percentiles).[42] Results were indicated as odds ratio (OR) with a 95% confidence interval (CI). Analyses were performed using GraphPad Prism software, statistical software SPSS version 24.0 (SPSS Inc., Chicago, IL, USA), and R version 3.6.1. *P* value < 0.05 was considered as statistically significant difference.

Role of the funders

The funders did not involve in study design, data collection, data analyses, interpretation of data, or writing of the report.

Results

Circulating Cav-1 level is associated with the early outcome of EVT patients

We firstly evaluated the clinical significance of Cav-1 in ischemic stroke patients. We prospectively recruited 270 stroke patients with successful recanalization by EVT (mean age, 68.4 ± 12.4 years; 63.3% male). One hundred patients (37.0%) experienced ENI during hospitalization. The baseline characteristic of the study sample stratified by the clinical outcome was demonstrated in Supplemental Table 2. Compared to patients with ENI, those without it had a reduced level of serum Cav-1 (Figure 1a). In addition, restricted cubic spline regression further confirmed a dose-response association of serum Cav-1 concentration with ENI (Figure 1b).

Among the 270 patients with EVT, 81 received MES evaluation by TCD monitoring. MES was detected in 35.8% of patients (29/81). Compared to patients without MES, those with it had a trend of reduced serum Cav-1 (Figure 1c). Furthermore, the Spearman correlation coefficient showed a negative trend between serum Cav-1

concentration and the number of MES in stroke patients after EVT treatment (Figure 1d).

Endothelial and serum Cav-1 levels are both decreased at tMCAO-24h

tMCAO steadily yielded about 31.7% infarct volume at 24 h post-surgery in our model (Supplemental Figure 1a and 1b). Neurological function was significantly destroyed, as the mNSS score climbed to 8.0 ± 1.1 (Supplemental Figure 1c). For the immunostaining image acquisition and analysis, eight fields in the peri-infarct region were chosen in every sample (Supplemental Figure 1d). We probed Cav-1 expression to examine whether Cav-1 was involved in tMCAO. Co-stained with CD31, immunostaining intensity of endothelial Cav-1 was remarkably reduced in the peri-infarct regions than in the sham-operated mice (Supplemental Figure 1e and 1f). In the extracted brain microvascular segments from the peri-infarct tissue, we confirmed the enrichment of endothelial cells through light microscopy and Claudin-5 expression (Supplemental Figure 1g–i). Immunoblotting of endothelial Cav-1 protein also showed a significant decline at tMCAO-24 h (Supplemental Figure 1j and 1k). Consistently, serum Cav-1 level was reduced to 0.75 ± 0.25 ng/mL 24 h after surgery (Supplemental Figure 1l). Regarding the important role of Cav-1 in caveolae maintenance,[43,44] we then determined whether the alteration of Cav-1 was associated with a change in caveolae. Through TEM assessment, we noted a concomitant loss of caveolae in the arteriole (Supplemental Figure 2a and 2b). Moreover, the expression of vascular PTRF, a selective marker for mature caveolae at the plasma membrane,[45] was likewise reduced in the peri-infarct area (Supplemental Figure 2c–f).

To validate the cell-type specificity of Cav-1 expression, we evaluated the *Cav-1* mRNA and protein expression in primary cultured microvascular endothelial cells, glial cells (OPCs, oligodendrocytes, microglia, and astrocytes), and neurons. *In vitro* analysis revealed that Cav-1 was mainly expressed by microvascular endothelial cells (Supplemental Figure 3a–c). *In vivo* staining disclosed that in physiological conditions about 80.7% of vascular endothelial cells ($CD31^+$), whose expression was significantly higher than other neural cells (Supplemental Figure 3d–g and 3j). Perivascular cells, including vascular smooth muscle cells (VSMCs) and pericytes, also expressed Cav-1 in normoxia (Supplemental Figure 3h–j). However, at 24 h after tMCAO, only the proportion of Cav-1 and CD31 co-positive cells significantly dropped. The level of Cav-1 in either pericytes or VSMCs was not statistically changed at tMCAO-24 h, suggesting that Cav-1 in pericytes and VSMCs might not be involved in the acute injury after tMCAO. Collectively, these results suggest that tMCAO-induced

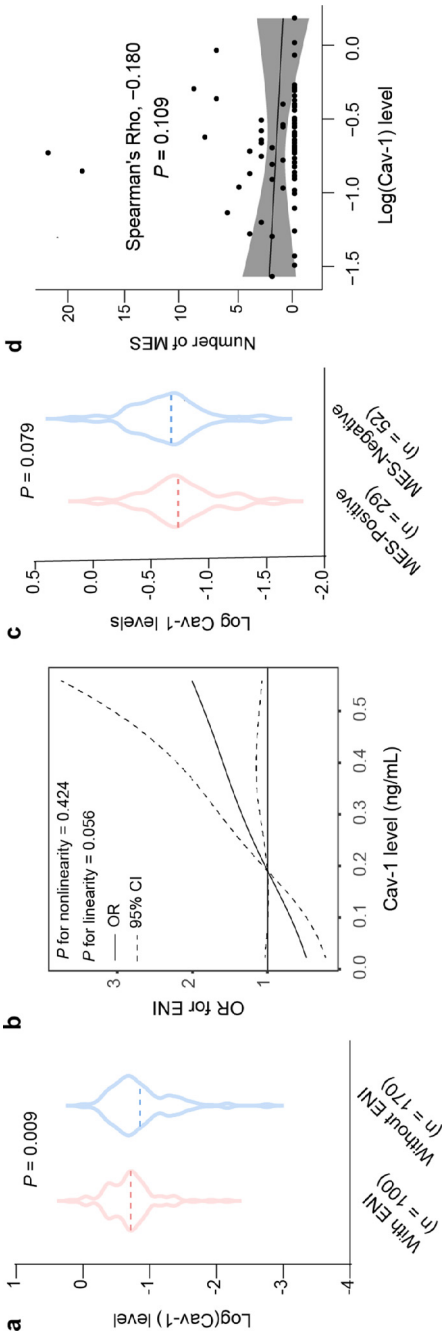

Figure 1. Association between serum Cav-1 and ENI or cerebral microembolic signals in ischemic stroke patients despite successful recanalization. (**a**) Comparison of the serum Cav-1 levels in patients with and without ENI. (**b**) A restricted cubic spline model was performed to explore the shape of the association between serum cav-1 and ENI, fitting a restricted cubic spline function with 3 knots (at 5th, 50th, and 95th percentiles). (**c**) Comparison of the serum Cav-1 levels in patients with and without positive MES. (**d**) Spearman's correlation analysis evaluated the association between serum cav-1 and the number of MES.

reduction of Cav-1 mostly resulted from endothelial Cav-1 loss in the peri-infarct area.

Cav-1 deficiency aggravates post-stroke infarction progression and microvascular breakdown

We firstly compared microvascular structure and permeability in *Cav-1*$^{-/-}$ mice with wild-type mice under normal conditions. The physiological parameters of WT and *Cav-1*$^{-/-}$ mice were demonstrated in Supplemental Table 3 and revealed no significant differences. The total and average length of Collagen IV and CD31 co-stained microvessels were significantly decreased in *Cav-1*$^{-/-}$ mice (Supplemental Figure 4a–c). However, no significant change was found in vessel density between wild-type and *Cav-1*$^{-/-}$ mice (Supplemental Figure 4d). As for microvascular permeability, mice with the deletion of Cav-1 exhibited slight extravasation of albumin around CD31^{+} microvessels (Supplemental Figure 4e and 4f), suggesting that Cav-1 was required not only in vasculature development but also in the endothelial barrier. To ask whether Cav-1 was involved in platelet adhesion, we used thrombocytes to label platelets and found a sparse deposition of platelets in brain microvessels (Supplemental Figure 4g and 4h). After tMCAO, invalidation of Cav-1 induced an enlarged infarct volume to 40.6% ± 2.0%, as defined by T2-weighted images (Supplemental Figure 5a and 5b). Consequently, *Cav-1*$^{-/-}$ tMCAO mice exhibited worse neurological function with a higher mNSS score and mortality 24 h after the surgery (Supplemental Figure 5c and Supplemental Table 3). To better depict the microscopic view of endothelial leakage, we combined albumin and IgG staining with CD31. The amount of extravasated albumin and IgG at the peri-infarct area was both substantially increased in tMCAO-treated *Cav-1*$^{-/-}$ mice (Supplemental Figure 5d–f). As evaluated by TEM, the morphology of TJ was significantly altered in *Cav-1*$^{-/-}$ tMCAO mice, characterized by an increased fraction of TJ with increased gaps than wild-type tMCAO mice (Supplemental Figure 5g–i). The level of TJ elements, such as zonula occludens-1 (ZO-1) and occludin, was significantly decreased under genetic ablation of *Cav-1* after tMCAO (Supplemental Figure 5j–p).

Cav-1 deficiency exacerbates post-stroke microvascular thrombo-inflammation

We performed thrombocyte and fibrinogen staining to display the presence of microvascular thrombi after cerebral I/R injury. As a result, *Cav-1*$^{-/-}$ tMCAO mice had more extensive co-localization of platelets, as well as fibrinogen, in CD31-positive microvessels at peri-infarct regions (Figure 2a–d). Furthermore, HE staining discovered that deletion of Cav-1 increased the percentage of occluded vessels by thrombi, which was averagely 2.46 times higher than wild-type mice subjected to tMCAO (Figure 2e and 2f). The FITC-dextran of 2000-kDa was used as a fluorescent tracer to illustrate the function of these seemingly occluded microvessels after tMCAO. As shown in Figure 2g and 2h, the number of perfused vessels was reduced by 1.7-fold in the peri-infarct region of *Cav-1*$^{-/-}$ tMCAO mice. Microvascular segments of the peri-infarct area were extracted and examined by immunoblotting to confirm the protein expression of thrombosis-related molecules, including vWF and plasminogen activator inhibitor-1 (PAI-1). As expected, these factors were both increased under Cav-1 deficiency (Figure 2i–k).

We next asked whether Cav-1 deletion could affect microvascular inflammation and immune cell recruitment under cerebral ischemic injury. The expression of microvascular ICAM-1 and VCAM-1 was markedly increased in the *Cav-1*$^{-/-}$ ischemic brain (Figure 3a–d). The protein level of adhesion molecules as well as inflammatory cytokines, including ICAM-1, VCAM-1, IL-1β, and TNF-α, was consistently up-regulated in *Cav-1*$^{-/-}$ microvessels (Figure 3e–i). Immunostaining and flow cytometry were then used to explore the adhesion and infiltration of immune cell recruitment. Dual-label immunofluorescence analyses demonstrated that the number of Ly6G^{+} neutrophils adhering to vessels and migrating to the parenchyma was increased in *Cav-1*$^{-/-}$ tMCAO mice than wild-type tMCAO mice 24 h after the surgery (Figure 3j and 3k). Illustrated by flow cytometry analysis (Supplemental Figure 6), *Cav-1*$^{-/-}$ microvessels allowed increased recruitment of myeloid cells (CD45^{high}CD11b^{high}) (Figure 3l–n). Of these infiltrating myeloid cells, neutrophils (CD45^{high}CD11b^{high}Ly6G^{+}) and monocytes (CD45^{high}CD11b^{high}Ly6C^{+}) were both increased, which were significantly higher in *Cav-1*$^{-/-}$ peri-infarct brains compared to wild-type mice (Figure 3o and 3p).

Specific expression of endothelial Cav-1 reduces infarct volume and thrombo-inflammation after cerebral I/R injury

To confirm the function of endothelial Cav-1 after tMCAO, we utilized a genetic approach to express Cav-1 specifically in endothelial cells. AAV-*Tie1*-GFP carrying cDNAs encoding control or *Cav-1* gene was stereotaxically injected into the lateral cerebral ventricle 3 weeks before tMCAO modeling (Figure 4a). Based on T2 images, specific restoration of endothelial Cav-1 significantly induced a reduction of infarct volume by 9.8% in wild-type tMCAO mice and by 7.7% in *Cav-1*$^{-/-}$ tMCAO mice (Supplemental Figure 7a and 7b). Importantly, reduced stroke size translated into improved functional outcomes as assessed by the mNSS score (Supplemental Figure 7c). Microscopically, under the *Tie1* promoter, the viruses with GFP signals were predominantly observed in CD31^{+} microvessels, whose Cav-1 level was

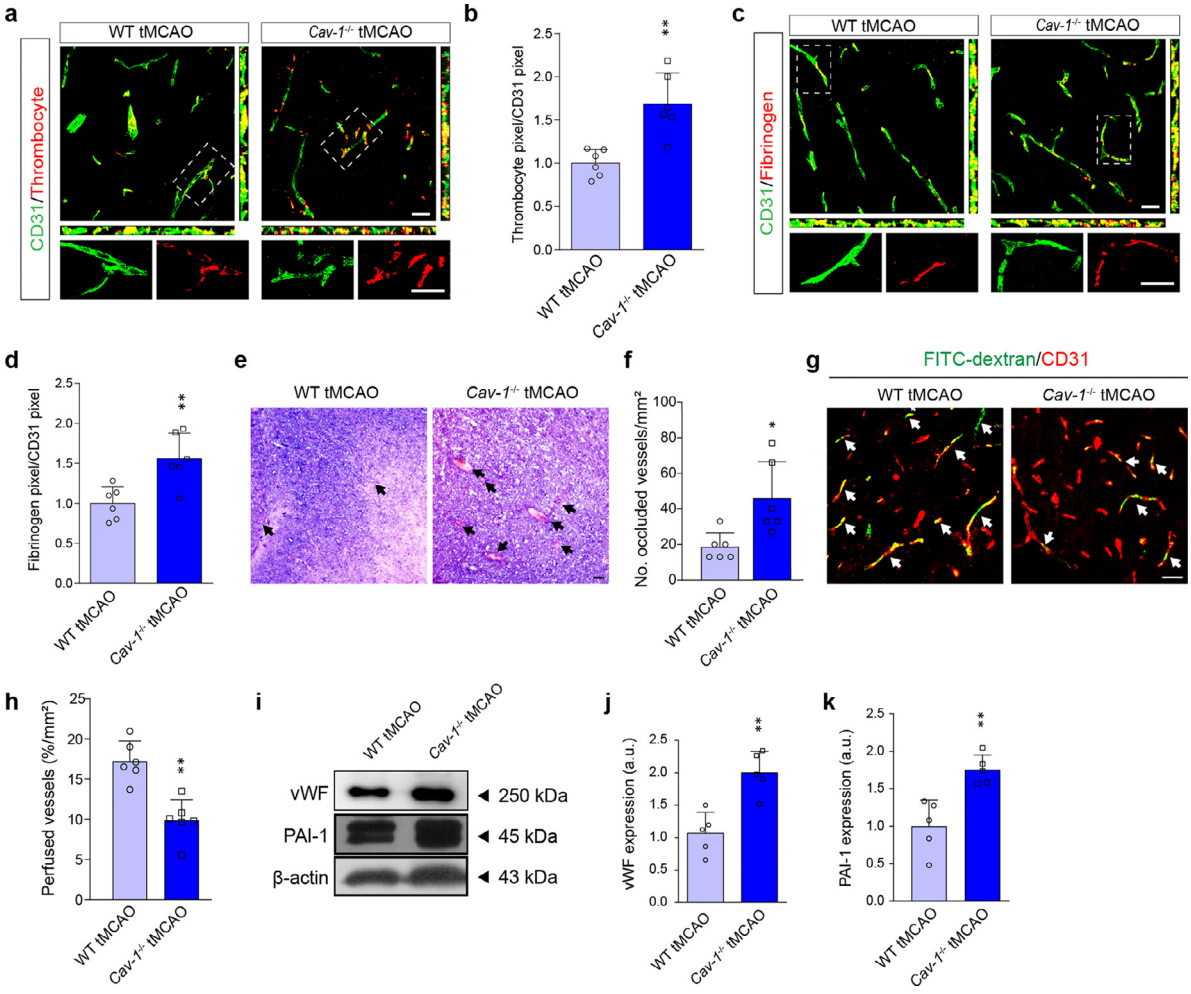

Figure 2. Cav-1 deficiency exacerbates the formation of microvascular thrombi 24 h after cerebral I/R injury. (**a, c**) Representative confocal images of thrombocytes (red) and fibrinogen (red) in the CD31$^+$ cerebral microvessels (green) in the peri-infarct area from WT and *Cav-1*$^{-/-}$ mice 24 h after tMCAO [quantified in (**b, d**); $n = 6$ in each group; mean ± S.D; $^{**}P < 0.01$ *vs.* WT tMCAO mice by unpaired t-test]. (**e, f**) HE staining and quantification showing occluded microvessels (indicated by black arrowheads) 24 h after the surgery. Results are expressed as the number of occluded vessels relative to the area ($n = 6$ in each group; mean ± S.D; $^{*}P < 0.05$ *vs.* WT tMCAO mice by unpaired t-test). (**g, h**) Representative images of immunofluorescence staining and quantification of FITC-dextran perfusion in the CD31$^+$ cerebral microvessels (red) 24 h post-stroke. Data are presented as the percentage of perfusion vessels relative to the area ($n = 6$ in each group; mean ± S.D; $^{**}P < 0.01$ *vs.* WT tMCAO mice by unpaired t-test). (**i**–**k**) Immunoblotting and quantification showing the expression of vWF and PAI-1 in brain microvessels from the peri-infarct region 24 h post-tMCAO (a pool of 2 mice per sample, $n = 5$ samples in each group; mean ± S.D; $^{**}P < 0.01$ *vs.* WT tMCAO mice by unpaired t-test). Scale bar: 20 μm. (For interpretation of the references to color in this figure legend, the reader is referred to the web version of this article.)

successfully increased by AAV-*Tie1-Cav-1* in wild-type and *Cav-1*$^{-/-}$ mice (Figure 4b–e). We then asked whether there was a change in the number of caveolae after the Cav-1 level was elevated. AAV-*Tie1-Cav-1* did not promote the formation of caveolae after I/R injury, as supported by the results of PTRF/CD31 staining that no significant differences were presented between the two AAV transfected groups of two genotypes (Supplemental Figure 8). Microvascular structure was resumed by TJ with smaller gaps after endothelial Cav-1 was restored (Figure 4f–h). TJ level of ZO-1 and occludin was also increased (Supplemental Figure 9). As a result, I/R-caused IgG leakage was substantially inhibited (Figure 4i and 4j).

We subsequently sought to determine whether specific over-expression of endothelial Cav-1 could attenuate post-stroke thrombo-inflammation. We noted that the amount of FITC-dextran-perfused microvessels at the peri-infarct area 24 h after tMCAO was substantially elevated by increased endothelial Cav-1 levels in both wild-type and *Cav-1*$^{-/-}$ tMCAO mice (Figure 5a and 5b). Compared to the null GFP reporter virus, AAV-*Tie1-Cav-1*

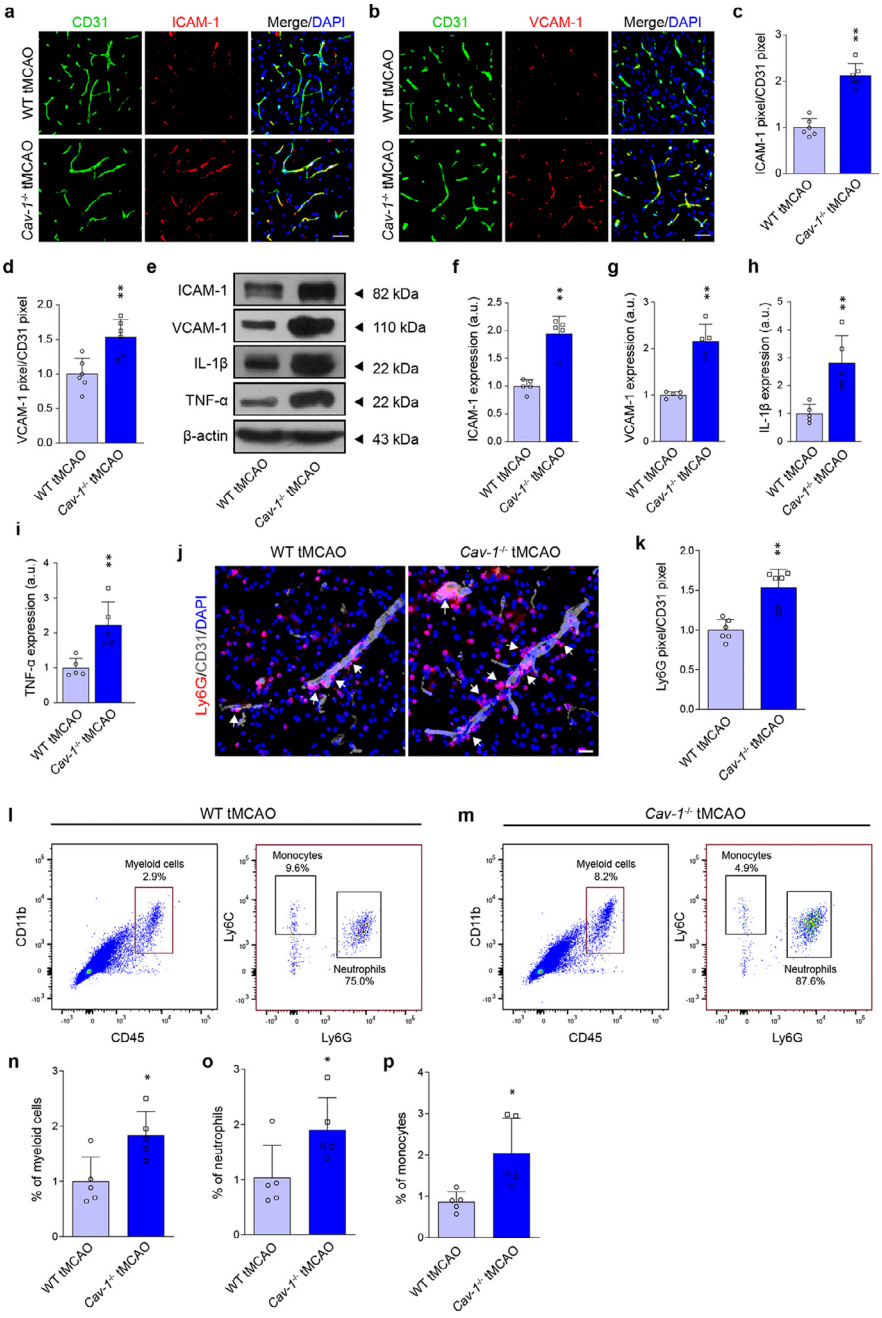

Figure 3. Cav-1 deficiency aggravates post-stroke microvascular inflammation and immune cell recruitment 24 h after tMCAO. (**a, b**) Representative immunofluorescent images showing the expression of microvascular ICAM-1 and VCAM-1 in the peri-infarct area of tMCAO mice of two genotypes 24 h after tMCAO [quantified in (**c, d**); $n = 6$ in each group; mean ± S.D; $^{**}P < 0.01$ *vs.* WT tMCAO mice by unpaired t-test]. (**e**–**i**) Immunoblotting and quantification showing the expression of ICAM-1, VCAM-1, TNF-α, and IL-1β in brain microvessels from the peri-infarct region 24 h after surgery (a pool of 2 mice per sample, $n = 5$ samples in each group; mean ± S.D; $^{**}P < 0.01$ *vs.* WT tMCAO mice by unpaired t-test). (**j, k**) Representative immunofluorescent images and quantification showing the $Ly6G^+$ cells adhering to $CD31^+$ vessels and migrated into the parenchyma at the peri-infarct area 24 h after tMCAO ($n = 6$ in each group; mean ± S.D; $^{**}P < 0.01$ *vs.* WT tMCAO mice by unpaired t-test). (**l, m**) Representative flow cytometry graphs showing myeloid cell infiltration in the ischemic hemisphere of WT tMCAO and *Cav-1*$^{-/-}$ tMCAO mice. High expression of CD45 and CD11b (upper right quadrant), indicative of myeloid cells, were further subdivided into Ly6G-positive neutrophils and Ly6C-positive monocytes [quantified in (**n**–**p**); $n = 5$ in each group; mean ± S.D; $^{*}P < 0.05$ *vs.* WT tMCAO mice by unpaired t-test)]. Scale bar: 20 μm.

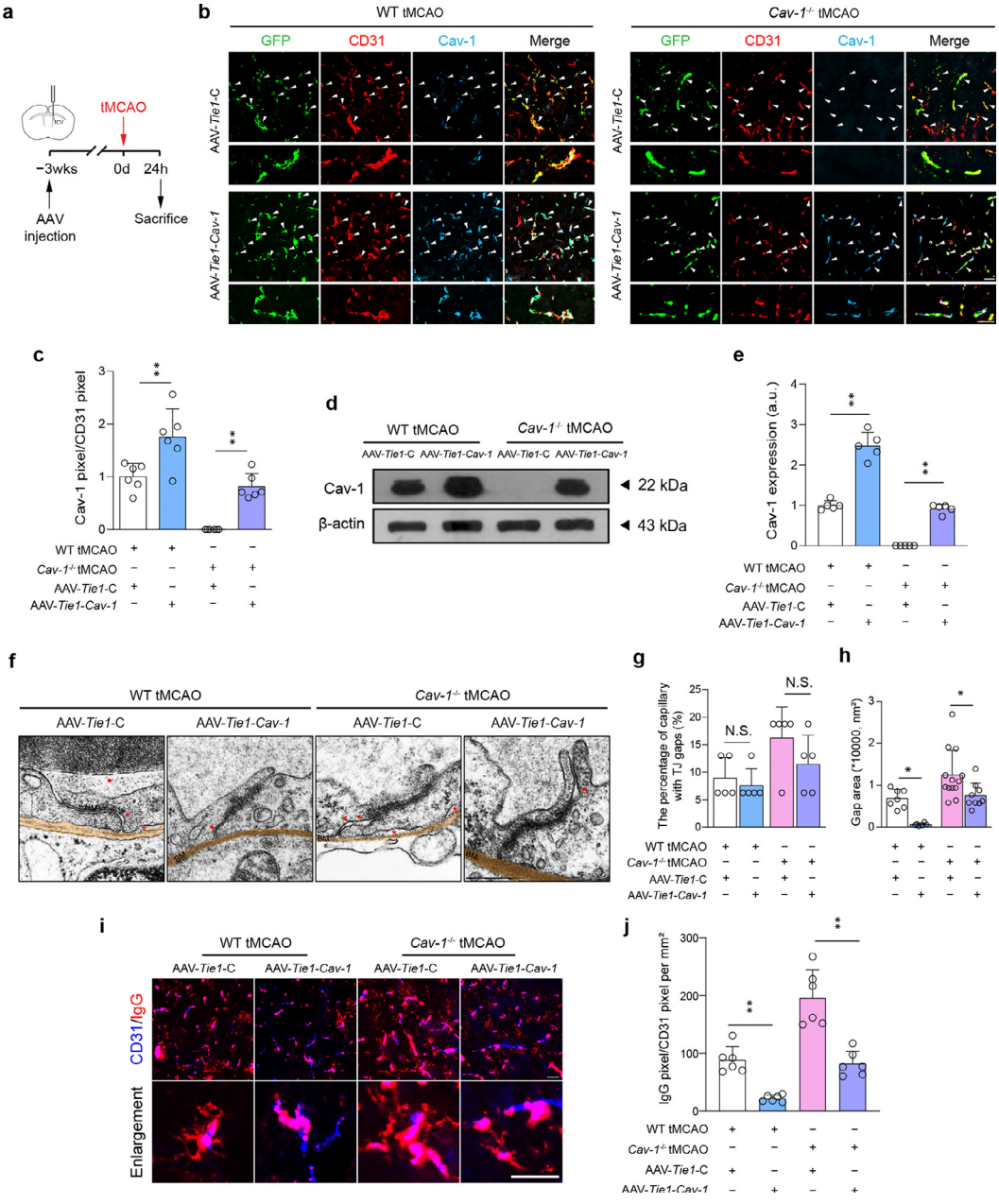

Figure 4. Specific enhanced expression of Cav-1 in endothelial cells attenuates microvascular breakdown at tMCAO-24 h. (**a**) Experimental flow chart. (**b**) Representative fluorescent images of transfection of AAV with GFP (green) reporter into CD31$^+$ microvessels (red) with enforced Cav-1 (light blue) expression at the peri-infarct tissue 24 h after surgery [quantified in (**c**); $n = 6$ in each group; mean ± S.D; $^{**}P < 0.01$ *vs.* AAV-*Tie1*-C-transfected mice by one-way ANOVA with Tukey post hoc test]. (**d, e**) Immunoblotting and quantification showing the expression of Cav-1 in microvascular segments of peri-infarct area 24 h after surgery (a pool of 2 mice per sample, $n = 5$ samples in each group; mean ± S.D; $^{**}P < 0.01$ *vs.* AAV-*Tie1*-C-transfected mice by one-way ANOVA with Tukey post hoc test). (**f**) TEM images and quantifications showing TJ gaps (red arrows) in the peri-infarct area [quantified in (**g, h**); $n = 5$ mice in each group. Sixteen capillaries were randomly chosen in each mouse; mean ± S.D; $^{*}P < 0.05$ *vs.* AAV-*Tie1*-C-transfected mice by one-way ANOVA with Tukey post hoc test]. The red arrows indicate gaps between endothelial cells. The red asterisks indicate gaps between endothelial cells and basal membrane. (**i-j**) Representative images and quantification showing the IgG leakage at the peri-infarct tissue ($n = 6$ in each group; mean ± S.D; $^{**}P < 0.01$ *vs.* AAV-*Tie1*-C-transfected mice by one-way ANOVA with Tukey post hoc test). Scale bar: 20 μm in (**b, i**) and 500 nm in (**f**). BM, basal membrane. (For interpretation of the references to color in this figure legend, the reader is referred to the web version of this article.)

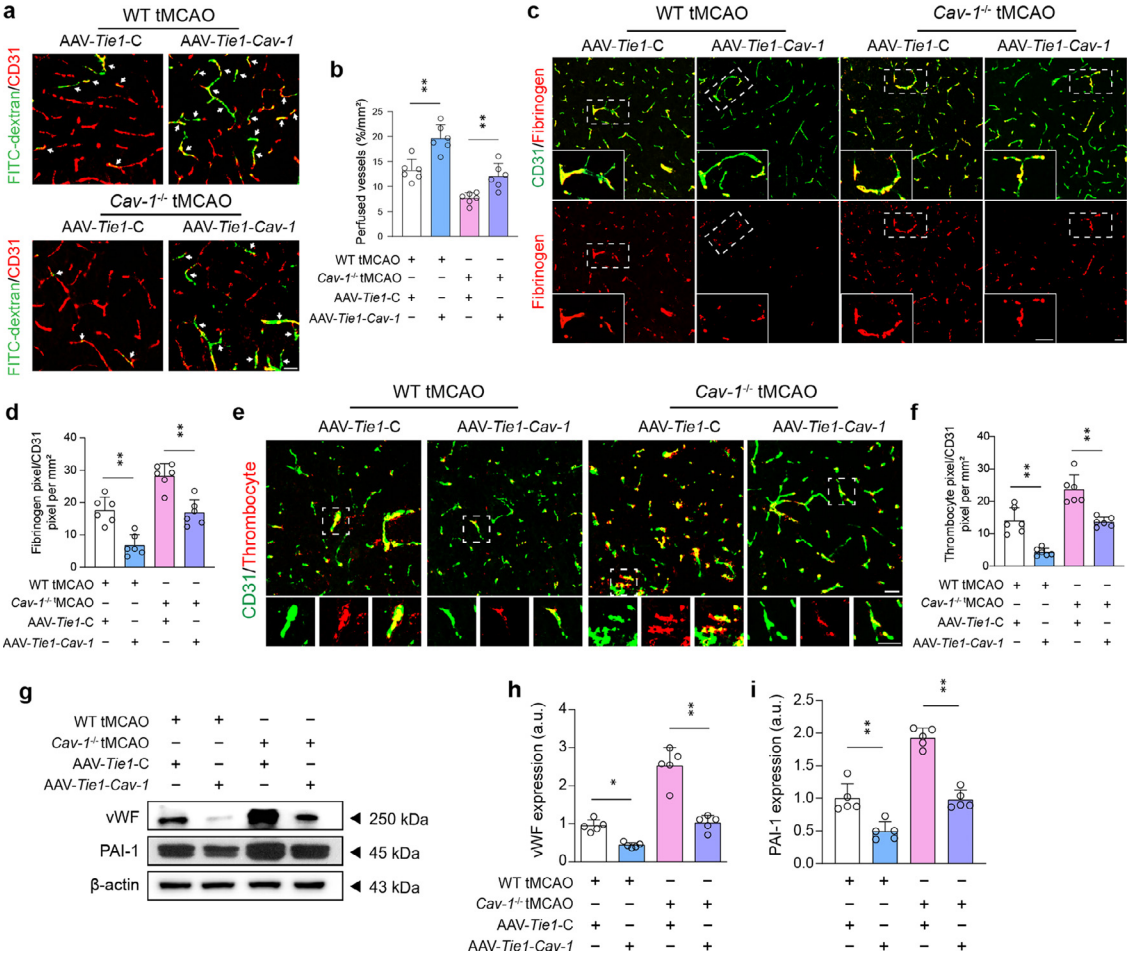

Figure 5. Specific enhanced expression of Cav-1 in endothelial cells ameliorates thrombus formation at tMCAO-24 h. (**a, b**) Representative images of immunofluorescence staining and quantification showing the FITC-dextran perfusion in the CD31$^+$ cerebral microvessels (red) at the peri-infarct tissue 24 h after surgery. Data are presented as the percentage of perfusion vessels relative to the imaged area (n = 6 in each group; mean ± S.D; $^{**}P < 0.01$ *vs.* AAV-*Tie1*-C-transfected mice by one-way ANOVA with Tukey post hoc test). (**c, e**) Representative images of immunofluorescence staining showing the positive for fibrinogen (red) and thrombocytes (red) in the CD31$^+$ cerebral microvessels (green) of the peri-infarct area 24 h after surgery [quantified in (**d, f**); n = 6 in each group; mean ± S.D; $^{**}P < 0.01$ *vs.* AAV-*Tie1*-C-transfected mice by one-way ANOVA with Tukey post hoc test]. Insets showing a higher magnification view. (**g**–**i**) Immunoblotting and quantification showing the expression of vWF and PAI-1 in microvascular segments of the peri-infarct region 24 h after surgery (a pool of 2 mice per sample, n = 5 samples in each group; $^{*}P < 0.05$, $^{**}P < 0.01$ *vs.* AAV-*Tie1*-C-transfected mice by one-way ANOVA with Tukey post hoc test). Scale bar: 20 μm. (For interpretation of the references to color in this figure legend, the reader is referred to the web version of this article.)

transfection suppressed the accumulation of fibrinogen and blood platelets in the microcirculation after I/R injury (Figure 5c–f), which may be resulted from the inhibited expression of endothelial vWF and PAI-1 (Figure 5g–i). Similarly, the enforced expression of endothelial Cav-1 profoundly reduced the recruitment of circulating myeloid cells by the attenuation of microvascular ICAM-1, and VCAM-1 level, and mitigated vascular inflammation by diminishing the generation of IL-1β and TNF-α (Figure 6). These findings suggest that endothelial Cav-1 could play a pivotal role in regulating cerebral thrombo-inflammation independent of caveolae.

Decreased endothelial Cav-1 contributes to the reduction of RXR-γ

To explore the downstream effector in Cav-1 function, high-throughput mRNA sequencing was employed. We screened out 15 mRNAs that were significantly altered (with a fold change >= 2) by the tMCAO model and were with a more significant fold change in *Cav-1*$^{-/-}$

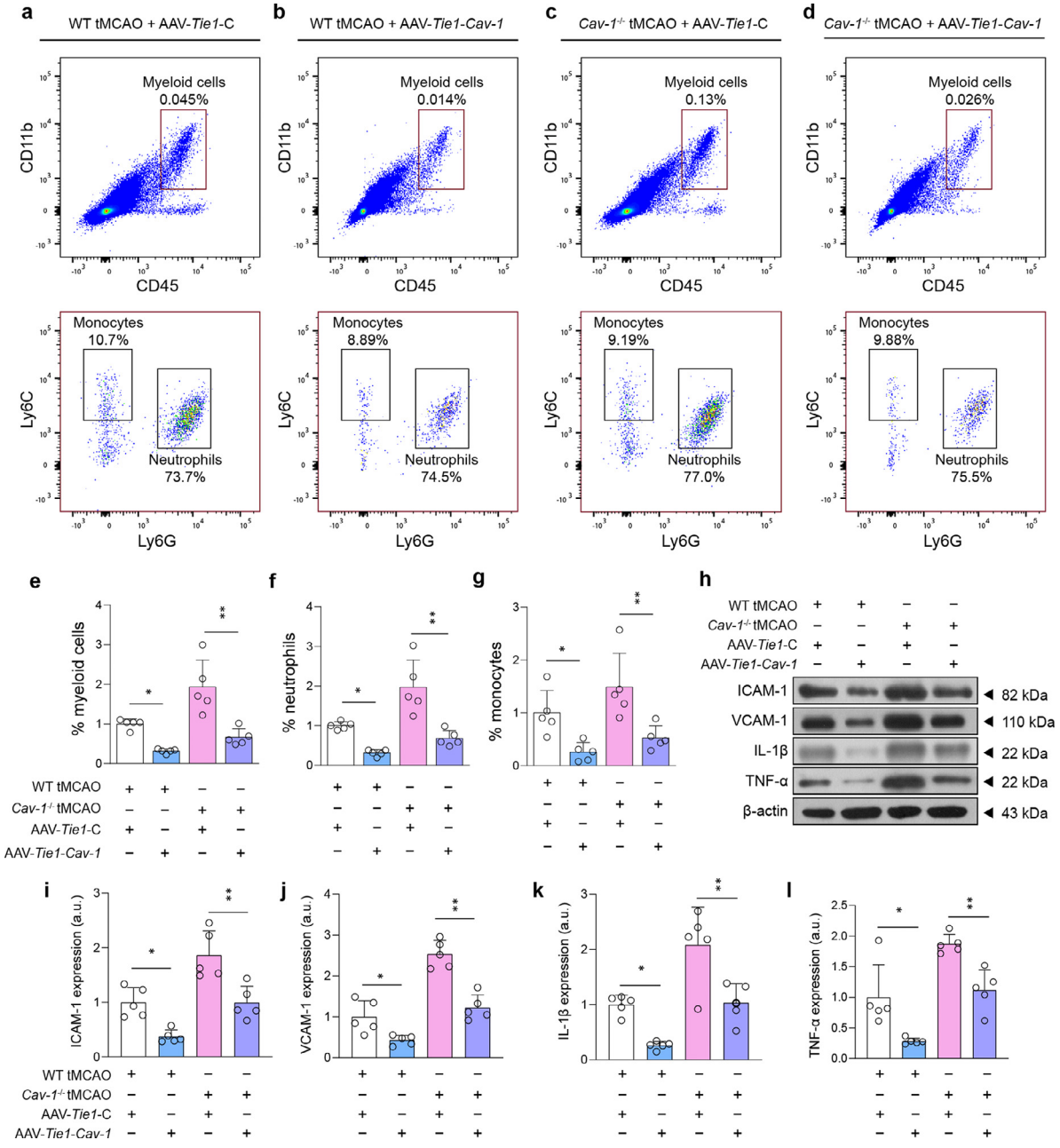

Figure 6. Specific enhanced expression of Cav-1 in endothelial cells reduces post-stroke immune cell recruitment at tMCAO-24 h. (**a**–**d**) Representative flow cytometry graphs showing the myeloid cell infiltration in the ischemic hemisphere of WT tMCAO and *Cav-1*$^{-/-}$ tMCAO mice pre-treated with AAV-*Tie1*-C or AAV-*Tie1-Cav-1*. High expression of CD45 and CD11b (upper right quadrant), indicative of infiltrated myeloid cells, were further subdivided into Ly6G-positive neutrophils and Ly6C-positive monocytes [quantified in (**e**–**g**); $n = 5$ in each group; mean ± S.D; $^{*}P < 0.05$, $^{**}P < 0.01$ *vs.* AAV-*Tie1*-C-transfected mice by one-way ANOVA with Tukey post hoc test). (**h**–**l**) Immunoblotting and quantifications showing the expression of ICAM-1, VCAM-1, TNF-α, and IL-1β in microvascular segments of peri-infarct area at tMCAO-24 h (a pool of 2 mice per sample, $n = 5$ samples in each group; $^{*}P < 0.05$, $^{**}P < 0.01$ *vs.* AAV-*Tie1*-C-transfected mice by one-way ANOVA with Tukey post hoc test).

tMCAO mice (Figure 7a). After excluding the altered mRNAs resulting from the genetic difference between wild-type and *Cav-1*$^{-/-}$ sham-operated mice, 11 mRNAs were chosen at the peri-infarct region (Figure 7b). Real-time PCR was used to confirm these data. Of note, compared to *Cav-1*$^{-/-}$ peri-infarct brain, *Rxrg* mRNA was the most significantly changed mRNA with an approximate reduction of 4.97-fold (Figure 7c–e). Besides, the

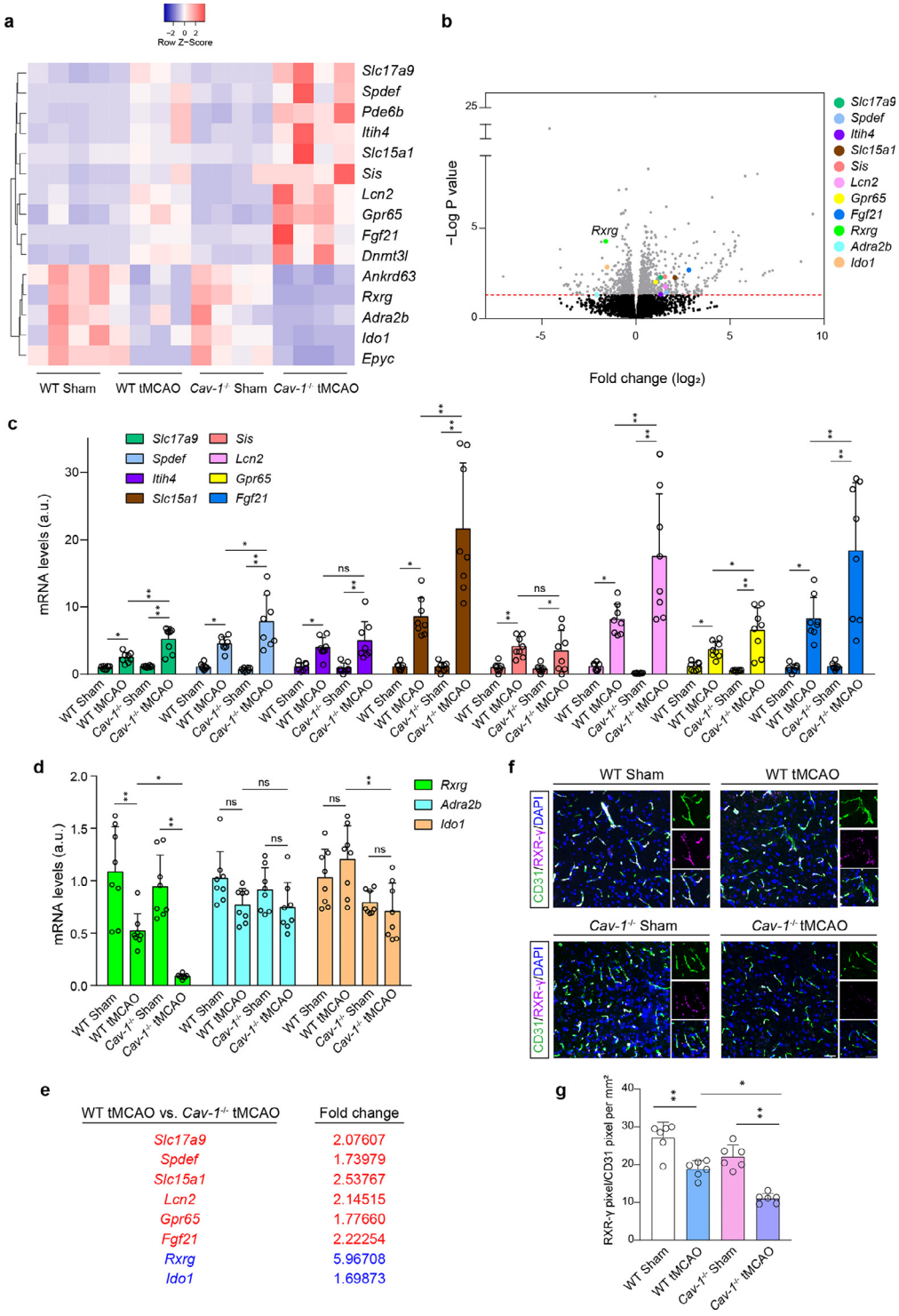

WT tMCAO vs. *Cav-1*$^{-/-}$ tMCAO	Fold change
Slc17a9	2.07607
Spdef	1.73979
Slc15a1	2.53767
Lcn2	2.14515
Gpr65	1.77660
Fgf21	2.22254
Rxrg	5.96708
Ido1	1.69873

Figure 7. Endothelial RXR-γ is significantly decreased in the peri-infarct area of *Cav-1*$^{-/-}$ tMCAO mice at 24 h. (**a, b**) Systematic screening of factors resultant from Cav-1 loss after tMCAO (n = 4 in each group). (**c**–**e**) Real-time PCR for validation of 11 mRNAs in the peri-infarct area (n = 8 experiments in each group; mean ± S.D; *P < 0.05, **P < 0.01 by one-way ANOVA with Tukey post hoc test). (**f**) Immunofluorescence staining showing the expression of RXR-γ (violet) in the CD31^{+} vascular endothelium (green) at the peri-infarct area of 4 groups at tMCAO-24 h [quantified in (**g**); n = 6 in each group; mean ± S.D; *P < 0.05, **P < 0.01 by one-way ANOVA with Tukey post hoc test]. Scale bar: 20 μm. N.S., no significance.

protein expression of microvascular RXR-γ was consistent with its mRNA level. Immunofluorescence demonstrated that cerebral RXR-γ was mostly expressed by $CD31^+$ microvessels. In mice subjected to tMCAO, microvascular RXR-γ was decreased, whose reduction was more significant under the Cav-1-deficient condition (Figure 7f and 7g).

We then introduced Cav-1 siRNA into wild-type mice to intuitively determine the relationship between Cav-1 and RXR-γ. N.C. or Cav-1 siRNA was intravenously injected in mice at intervals of three days for five injections (Supplemental Figure 10a). A robust uptake of Cy5-labeled N.C. and Cav-1 siRNA was captured in the microvessels (Supplemental Figure 10b). Compared to mice injected with N.C. siRNA, mice that received Cav-1 siRNA exhibited significantly lower expression of endothelial Cav-1 and RXR-γ (Supplemental Figure 10c–e). Similar results were obtained by immunoblotting for the extracted brain microvessels (Supplemental Figure 10f–h). These data collectively suggest that Cav-1 reduction could lead to RXR-γ decrease, which may function as a downstream effector of endothelial Cav-1 in cerebral I/R injury.

RXR-γ is an important intermediary in Cav-1-induced protection in cerebral I/R injury

Given the upstream regulation of Cav-1 on RXR-γ in cerebral microvessels, we asked whether suppression of RXR-γ could overcome the AAV-*Tie1-Cav-1*-induced salutary effects after tMCAO. N.C. or RXR-γ siRNA was injected every three days for five injections, starting at one week after AAV-*Tie1-Cav-1* transfection (Figure 8a). Compared to N.C. siRNA, RXR-γ siRNA aggravated neurological deficits with increased mNSS score in tMCAO mice transfected with AAV-*Tie1-Cav-1* (Figure 8b). Microscopically, the microvascular capture of Cy5-labeled N.C. or RXR-γ siRNA was identified in the peri-infarct brain (Figure 8c). RXR-γ siRNA markedly reduced RXR-γ expression, but did not affect microvascular Cav-1 level increased by AAV-*Tie1-Cav-1* (Figure 8d–f). Similarly, the PTRF expression was not altered (Supplemental Figure 11). As shown in Figure 8g–j, administration of RXR-γ siRNA exacerbated the adhesion of thrombocytes as well as fibrinogen in the microvessels, which were once ameliorated by enhanced expression of endothelial Cav-1. Additionally, RXR-γ knockdown reversed Cav-1-induced inhibition on myeloid cell infiltration. As illustrated by Ly6G and Ly6C staining, the number of leukocytes was significantly increased at the peri-infarct tissue in RXR-γ siRNA-treated tMCAO mice, though endothelial Cav-1 was rescued (Figure 8k–m). Elevated protein expression of thrombo-inflammation-related molecules was also detected in tMCAO mice receiving RXR-γ siRNA (Figure 8n–t). Most importantly, knockdown of RXR-γ did not induce any effects on endothelial TJ with gaps and TJ proteins expression (Supplemental Figure 12), suggesting that the RXR-γ might not be involved in manipulating microvascular hyper-permeability.

Discussion

Endothelial Cav-1 has been well-characterized in maintaining microvascular homeostasis. This study opens a new area of research on the role of Cav-1 in cerebral thrombo-inflammation. A positive and significant correlation existed between reduced serum Cav-1 and poor outcomes in acute ischemic stroke patients with successful EVT treatment. In tMCAO mice, acute cerebral I/R injury reduced endothelial Cav-1 as well as circulating Cav-1. Specific enhanced expression of endothelial Cav-1 inhibited infarct growth, rescued endothelial breakdown, and attenuated thrombo-inflammation independent of caveolae reservation. The consistent findings in the cohort and the animal study indicate the possibility of translation of laboratory findings to human biology. As the most significant downstream effector of Cav-1, RXR-γ selectively manipulated cerebral thrombo-inflammation, as knockdown of RXR-γ reversed Cav-1-induced suppression on the microthrombus formation and vascular inflammation without affecting microvascular TJ expression. Taken together, though endothelial Cav-1 per se was strongly involved in the integrated microvascular function, its downstream RXR-γ may be a specific regulator for cerebral thrombo-inflammation after acute I/R injury.

Both animal studies[46,47] and the clinical trial[48] concluded that anti-platelet aggregation was not effective to delay/stop stroke progression after recanalization. Therefore, a simple secondary thrombotic event could not explain post-stroke reperfusion injury. The closely intertwined action of thrombotic, as well as inflammatory mechanisms, may concertedly drive post-ischemic cerebral infarct progression, leading to the tempting concept of ischemic stroke being a thrombo-inflammatory disease.[8] Numerous attempts have been conducted to find novel targets engaged in the thrombo-inflammatory activity for stroke treatment. The plasma fibronectin-splicing variant containing extra domain A[49,50] and plasma kallikrein[51] were recently recognized as systemic targets for thrombo-inflammation and potential stroke therapies. Some investigations have reported that targeting platelet Glycoprotein Ib[17,21,52] and platelet AnxA1[53] was effective in ameliorating vascular occlusion, inhibiting inflammatory cell recruitment, and reducing post-stroke tissue damage. It is remarkable to note that endothelial dysfunction is the early prerequisite of thrombo-inflammatory events in cerebral I/R injury. Intact endothelium regulates vascular tone and maintains vascular homeostasis, including normal permeability and non-inflammatory, anti-thrombotic surface.[54] After the ischemic injury, thrombus formation and pro-

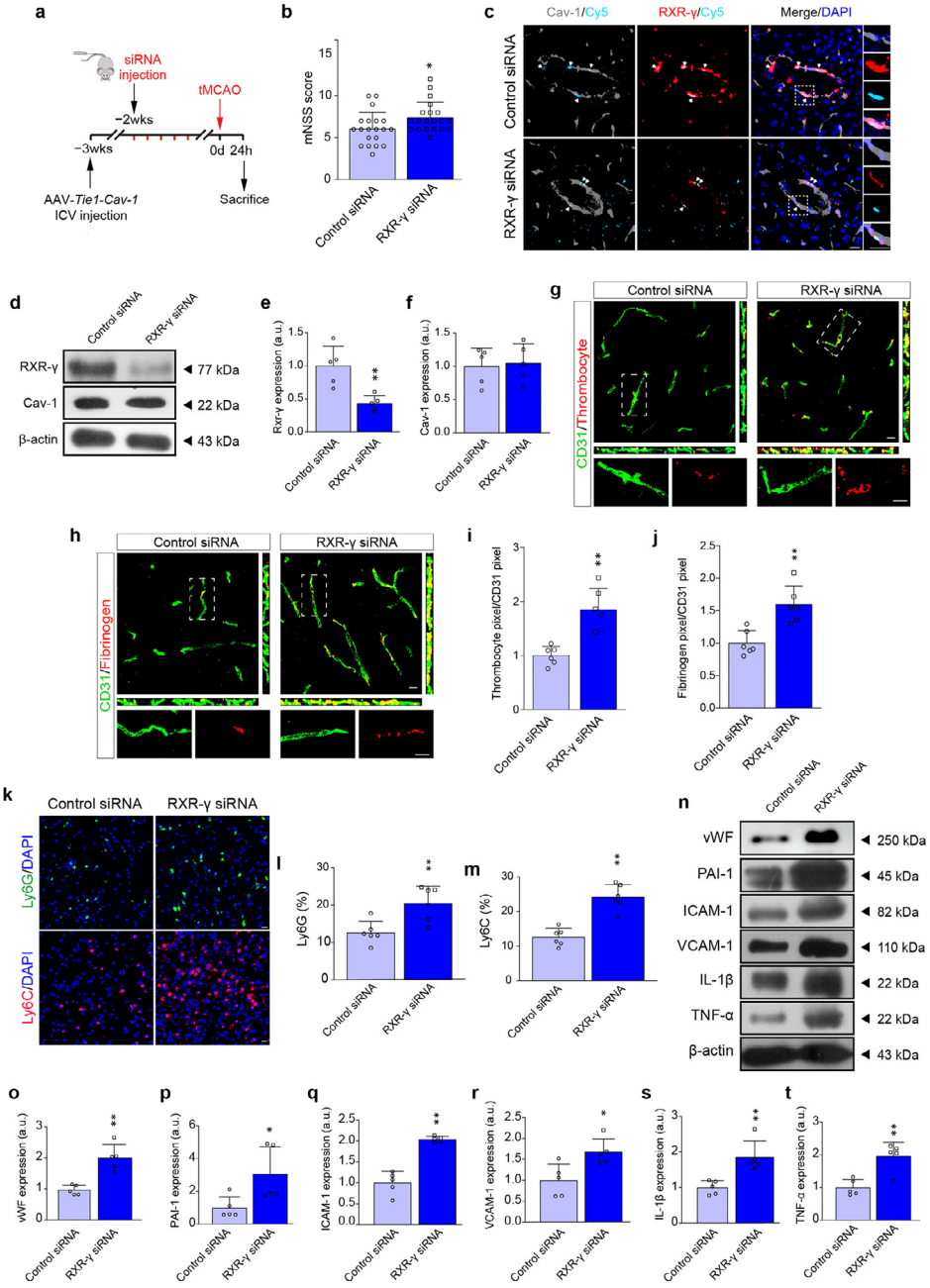

Figure 8. RXR-γ is required in Cav-1-induced protection in cerebral I/R injury at 24 h. (**a**) Experimental flow chart. (**b**) The mNSS score of control or RXR-γ siRNA-transfected wild-type tMCAO mice at 24 h (n = 20 in each group; mean ± S.D; *$P < 0.05$ *vs.* control siRNA-injected mice by unpaired t-test). (**c**) Representative images showing the co-localization of siRNA (cyan), RXR-γ (red) and cav-1 (gray). (**d**–**f**) Immunoblotting and quantifications showing the expression of RXR-γ and Cav-1 in the microvascular segments 24 h after surgery (a pool of 2 mice per sample, n = 5 samples in each group; **$P < 0.01$ *vs.* control siRNA-injected mice by unpaired t-test). (**g, h**) Representative orthogonal views of Z-stack images showing the fibrinogen (red) and thrombocyte (red) in the CD31$^+$ cerebral microvessels (green) 24 h after tMCAO [quantified in (**i, j**); n = 6 in each group; mean ± S.D; **$P < 0.01$ *vs.* control siRNA-treated mice by unpaired t-test]. (**k**) Representative immunofluorescent images showing the recruitment of Ly6G$^+$ neutrophils and Ly6C$^+$ monocytes at the peri-infarct area 24 h after tMCAO [quantified in (**l, m**); n = 6 in each group; mean ± S.D; **$P < 0.01$ *vs.* control siRNA-treated mice by unpaired t-test). (**n**–**t**) Immunoblotting and quantification showing the expression of vWF, PAI-1, ICAM-1, VCAM-1, TNF-α and IL-1β in brain microvascular segments 24 h after tMCAO (a pool of 2 mice per sample, n = 5 samples in each group; *$P < 0.05$, **$P < 0.01$ *vs.* control siRNA-injected mice by unpaired t-test). Scale bar: 10 μm. (For interpretation of the references to color in this figure legend, the reader is referred to the web version of this article.)

inflammatory action concomitantly take place at the sites of damaged or activated endothelial cells.[55]

Cav-1 is a ~20-kDa protein that is required for the formation of caveolae.[56] It has been reported to express in all types of cells in the CNS.[57] According to our data, tMCAO-induced Cav-1 reduction was dominantly found in endothelial cells of the peri-infarct brain 24 h after the surgery. Firstly, the reduction might be attributed to the inhibition of Cav-1 expression. Dysregulation of non-coding RNAs, including microRNAs and circular RNAs, has been found in the pathophysiology of cerebral vascular endothelium in the brain's response to ischemic stimuli.[58,59] In the ischemic stroke model, the level of miR-126, miR-98, circ-Memo1, and circ-DLGAP4 were reported to be altered in vascular endothelial cells.[60–63] Meanwhile, these non-coding RNAs could regulate Cav-1 expression by potentially targeting the 3' UTR region of *Cav-1* mRNA. Secondly, the reduction might be attributed to an increase in Cav-1 degradation. Reactive oxygen species after stroke onset could activate ZNRF1, which could promote Cav-1 ubiquitination and degradation.[64] Consistently, a previous study on the rat tMCAO model obtained similar results of decreased Cav-1 expression at 24 h in the ipsilateral hemisphere.[24] Other preclinical studies, on the contrary, have reported an increased Cav-1 level after ischemic insult.[65–67] This Cav-1 elevation was reported at either the hyperacute phase of MCAO-12h[67] or the chronic phase of MCAO-48h, MCAO-72h, or even 2 weeks post-ischemia.[65,66] The discrepancy could be explained by a time-course change of Cav-1 expression after stroke. It was reported that the level of Cav-1 was upregulated between 6 and 12 h, and decreased between 12 and 24 h, while increased again between 24 and 48 h post-tMCAO.[68] Other variations in the experimental protocols, such as the stroke model, the occlusion time, the methods evaluating Cav-1, and different ways of quantification, should also be taken into consideration. Cav-1 could act as an important mediator of anti-inflammatory effects by inhibiting the expression of the proinflammatory cytokine, such as Nuclear Factor-κB (NF-κB) and Activating Protein-1, and inducing the production of the anti-inflammatory cytokine, such as IL-10.[69] Furthermore, the Cav-1-dependent TLR4-MyD88-NF-κB pathway in endothelial cells could regulate endothelial barrier breakdown,[25] which could in turn exacerbate the inflammation after stroke. However, except for mediating inflammatory responses, little is known about the potential mechanism underlying the involvement of endothelial Cav-1 in thrombo-inflammation in the context of ischemic stroke. In our study, genetic delivery of AAV-*Tie1-Cav-1* was introduced, aiming to enhance Cav-1 expression exclusively in endothelial cells. AAV-*Tie1-Cav-1* reduced microvascular breakdown via reservation on TJ protein, which was in accordance with previously published literature.[70,71] Furthermore, microthrombi, represented by fibrinogen deposition and platelet adhesion, and neutrophil infiltration were remarkably attenuated by AAV-*Tie1-Cav-1*, suggesting an endothelial cell-autonomous function of Cav-1 on microvasculature and thrombo-inflammation. Consistent with the previous study,[72] over-expression of Cav-1 did not contribute to an increase in caveolae number, suggesting that the role of Cav-1 in thrombo-inflammation might be independent of the caveolae organelle. Therefore, our data suggest that the protection induced by increased Cav-1 may be ascribed to the regulatory function of non-caveolar Cav-1.

Downstream of endothelial Cav-1, we identified RXR-γ as an important factor generated from microvascular endothelium. RXR-γ was reported to be abundantly expressed in the CNS.[73,74] RXR-γ signaling is a critical regulator of CNS homeostasis, such as controlling behavioral abnormalities[75] and promoting remyelination.[76] We further broadened the effects of RXR-γ in the field of brain ischemic injury. Acute cerebral I/R injury decreased *Rxrg* mRNA and protein levels in the peri-infarction area. A more prominent decrease of RXR-γ was observed with the ablation of *Cav-1* under tMCAO conditions. Moreover, knockdown of RXR-γ could overcome the salutary effects of Cav-1, indicating RXR-γ may be an important downstream executor of endothelial Cav-1. RXR-γ was implicated in microthrombus formation, as RXR-γ siRNA induced upregulation of endothelial vWF and PAI-1 and permitted in situ aggregations of fibrinogen with platelets. We also found that RXR-γ knockdown could exaggerate inflammatory response by promoting endothelial expression of adhesion molecules (VCAM-1 and ICAM-1) and inflammatory cytokines (IL-1β and TNF-α), which may be corrected by the findings from RXR agonist.[77] Therefore, we speculated that Cav-1 may regulate cerebral thrombo-inflammation through the RXR-γ signaling in microvascular endothelial cells. Mechanistically, RXR, as a transcription factor, is known to form heterodimers with different nuclear receptors, such as peroxisome proliferator-activated receptors (PPARs). Except for regulating different metabolic pathways,[78] the PPAR-RXR heterodimeric complex is also reported to be involved in vascular biology, including anti-clotting through inhibiting endothelial thromboxane receptors[79,80] and controlling inflammatory responses.[80,81] Therefore, acute ischemia-induced disruption in Cav-1 expression decreased RXR-γ, which may then destroy the anti-thrombo-inflammation of stable heterodimers composed of RXR-γ.

However, several limitations should be addressed in the present study. Firstly, all outcomes in tMCAO mice and stroke patients with EVT were measured at 24 h. This time point was chosen to specifically investigate the early and acute thrombo-inflammatory response after stroke. Studies are needed to investigate the development of thrombo-inflammation at later time points. Secondly, the global *Cav-1*$^{-/-}$ mice were used, causing

Cav-1 depletion before tMCAO. Though Cav-1 was dominantly expressed and changed in endothelial cells, other cells expressing Cav-1 cannot be excluded. Thirdly, systemic siRNA delivery was not with high specificity. Perivascular uptake of off-target siRNA may exert confounding effects. Taken together, the results should be treated and interpreted with caution.

In summary, we showed a new mechanism engaging in cerebral thrombo-inflammation. Regulation of this complex interplay between blood coagulation and inflammation could prevent infarct development and alleviate tissue damage. In cerebral I/R injury, specific regulation of endothelial Cav-1/RXR-γ controlled the microvascular expression of molecules involved in thrombus formation and inflammatory action. As such, our study may shed light on a specific role of endothelial Cav-1/RXR-γ signaling in diseases involving thrombo-inflammatory circuits.

Contributors

G.X. and Y. Xie conceived and supervised the study. Y. Xie and X.Z. designed the research and wrote the manuscript. X.Z., Y.Z. and P.G. carried out the animal and the cellular experiments. T.W., K.Y., Y.Xiong, M.W. and Y.L. assisted with imaging experiments and image reconstruction. X.Z., Y.Z., P.G., and M.Z. recruited the patients and collected clinical samples. T.J., X.L. and R. Y. who were blinded to the group information, analyzed the data. G.X. and Y. Xie have accessed and verified the underlying data. All authors have read and approved the final version of the manuscript.

Data sharing statement

All relevant data are available within the manuscript and the Supplementary Materials. Requests for materials should be addressed to X.Y. (xy_307@126.com) or G.X. (gelinxu@nju.edu.cn).

Declaration of interests

The authors declare no potential conflicts of interest.

Acknowledgments

This work was supported by the National Natural Science Foundation of China (NSFC; No. 82171330 to G.X., No. 82171331 to Y.Xie., No. 82171272 to Y. Xiong., and No. 81901248 to X.Z.).

Supplementary materials

Supplementary material associated with this article can be found in the online version at doi:10.1016/j.ebiom.2022.104275.

References

1 Vos T, Barber RM, Bell B, et al. Global, regional, and national incidence, prevalence, and years lived with disability for 301 acute and chronic diseases and injuries in 188 countries, 1990–2013: a systematic analysis for the global burden of disease study 2013. *Lancet*. 2015;386(9995):743–800.
2 Shi Z, Liebeskind D, Xiang B, et al. Predictors of functional dependence despite successful revascularization in large-vessel occlusion strokes. *Stroke*. 2014;45(7):1977–1984.
3 Goyal M, Menon BK, van Zwam WH, et al. Endovascular thrombectomy after large-vessel ischaemic stroke: a meta-analysis of individual patient data from five randomised trials. *Lancet*. 2016;387(10029):1723–1731.
4 Zhang X, Yuan K, Wang H, et al. Nomogram to predict mortality of endovascular thrombectomy for ischemic stroke despite successful recanalization. *J Am Heart Assoc*. 2020;9(3):e014899.
5 Stoll G, Nieswandt B. Thrombo-inflammation in acute ischaemic stroke - implications for treatment. *Nat Rev Neurol*. 2019;15(8):473–481.
6 Desilles J, Syvannarath V, Di Meglio L, et al. Downstream microvascular thrombosis in cortical venules is an early response to proximal cerebral arterial occlusion. *J Am Heart Assoc*. 2018;7(5):e007804.
7 Schuhmann MK, Stoll G, Bieber M, et al. Cd84 links t cell and platelet activity in cerebral thrombo-inflammation in acute stroke. *Circ Res*. 2020;127(8):1023–1035.
8 Nieswandt B, Kleinschnitz C, Stoll G. Ischaemic stroke: a thrombo-inflammatory disease? *J Physiol*. 2011;589(17):4115–4123.
9 Li Z, Delaney MK, O'Brien KA, Du X. Signaling during platelet adhesion and activation. *Arterioscler Thromb Vasc Biol*. 2010;30(12):2341–2349.
10 Stoll G, Kleinschnitz C, Nieswandt B. Molecular mechanisms of thrombus formation in ischemic stroke: novel insights and targets for treatment. *Blood*. 2008;112(9):3555–3562.
11 Jackson SP, Darbousset R, Schoenwaelder SM. Thromboinflammation challenges of therapeutically targeting coagulation and other host defense mechanisms. *Blood*. 2019;133(9):906–918.
12 De Meyer SF, Denorme F, Langhauser F, et al. Thromboinflammation in stroke brain damage. *Stroke*. 2016;47(4):1165–1172.
13 del Zoppo GJ, Mabuchi T. Cerebral microvessel responses to focal ischemia. *J Cereb Blood Flow Metab*. 2003;23(8):879–894.
14 Iadecola C, Buckwalter MS, Anrather J. Immune responses to stroke: mechanisms, modulation, and therapeutic potential. *J Clin Invest*. 2020;130(6):2777–2788.
15 Eltzschig HK, Eckle T. Ischemia and reperfusion–from mechanism to translation. *Nat Med*. 2011;17(11):1391–1401.
16 Göb E, Reymann S, Langhauser F, et al. Blocking of plasma kallikrein ameliorates stroke by reducing thromboinflammation. *Ann Neurol*. 2015;77(5):784–803.
17 Schuhmann MK, Guthmann J, Stoll G, et al. Blocking of platelet glycoprotein receptor ib reduces "thrombo-inflammation" in mice with acute ischemic stroke. *J Neuroinflammation*. 2017;14(1):18.
18 Jin R, Xiao A, Chen R, et al. Inhibition of cd147 (cluster of differentiation 147) ameliorates acute ischemic stroke in mice by reducing thromboinflammation. *Stroke*. 2017;48(12):3356–3365.
19 Pober JS, Sessa WC. Evolving functions of endothelial cells in inflammation. *Nat Rev Immunol*. 2007;7(10):803–815.
20 Kleinschnitz C, Kraft P, Dreykluft A, et al. Regulatory t cells are strong promoters of acute ischemic stroke in mice by inducing dysfunction of the cerebral microvasculature. *Blood*. 2013;121(4):679–691.
21 Li J, Kim K, Jeong SY, et al. Platelet protein disulfide isomerase promotes glycoprotein ibalpha-mediated platelet-neutrophil interactions under thromboinflammatory conditions. *Circulation*. 2019;139(10):1300–1319.
22 Rothberg K, Heuser J, Donzell W, et al. Caveolin, a protein component of caveolae membrane coats. *Cell*. 1992;68(4):673–682.
23 Jasmin J, Malhotra S, Singh DM, et al. Caveolin-1 deficiency increases cerebral ischemic injury. *Circ Res*. 2007;100(5):721–729.
24 Gu Y, Zheng G, Xu M, et al. Caveolin-1 regulates nitric oxide-mediated matrix metalloproteinases activity and blood-brain barrier permeability in focal cerebral ischemia and reperfusion injury. *J Neurochem*. 2012;120(1):147–156.
25 Tiruppathi C, Shimizu J, Miyawaki-Shimizu K, et al. Role of nf-kappab-dependent caveolin-1 expression in the mechanism of increased endothelial permeability induced by lipopolysaccharide. *J Biol Chem*. 2008;283(7):4210–4218.

26 Yang Y, Rosenberg G. Blood-brain barrier breakdown in acute and chronic cerebrovascular disease. *Stroke*. 2011;42(11):3323–3328.
27 Zhang J, Zhu W, Xiao L, et al. Lower serum caveolin-1 is associated with cerebral microbleeds in patients with acute ischemic stroke. *Oxid Med Cell Longev*. 2016;2016:9026787.
28 Castellanos M, van Eendenburg C, Gubern C, et al. Low levels of caveolin-1 predict symptomatic bleeding after thrombolytic therapy in patients with acute ischemic stroke. *Stroke*. 2018;49(6):1525–1527.
29 Zhang X, Ramírez C, Aryal B, et al. Cav-1 (caveolin-1) deficiency increases autophagy in the endothelium and attenuates vascular inflammation and atherosclerosis. *Arterioscler Thromb Vasc Biol*. 2020;40(6):1510–1522.
30 Cerecedo D, Martínez-Vieyra I, Maldonado-García D, et al. Association of membrane/lipid rafts with the platelet cytoskeleton and the caveolin py14: participation in the adhesion process. *J Cell Biochem*. 2015;116(11):2528–2540.
31 Xu P, Zhang X, Liu Q, et al. Microglial trem-1 receptor mediates neuroinflammatory injury via interaction with syk in experimental ischemic stroke. *Cell Death Dis*. 2019;10(8):555.
32 Xu P, Liu Q, Xie Y, et al. Breast cancer susceptibility protein 1 (brca1) rescues neurons from cerebral ischemia/reperfusion injury through nrf2-mediated antioxidant pathway. *Redox Biol*. 2018;18:158–172.
33 Chen J, Li Y, Wang L, et al. Therapeutic benefit of intravenous administration of bone marrow stromal cells after cerebral ischemia in rats. *Stroke*. 2001;32(4):1005–1011.
34 Ruck T, Bittner S, Epping L, Herrmann AM, Meuth SG. Isolation of primary murine brain microvascular endothelial cells. *J Vis Exp*. 2014:(93):e52204.
35 Franklin RJM, Ffrench-Constant C. Regenerating cns myelin-from mechanisms to experimental medicines. *Nat Rev Neurosci*. 2017;18(12):753–769.
36 Eustace B, Sakurai T, Stewart J, et al. Functional proteomic screens reveal an essential extracellular role for hsp90 alpha in cancer cell invasiveness. *Nat Cell Biol*. 2004;6(6):507–514.
37 Xie Y, Guo H, Wang L, et al. Human albumin attenuates excessive innate immunity via inhibition of microglial mincle/syk signaling in subarachnoid hemorrhage. *Brain Behav Immun*. 2017;60:346–360.
38 Ashwal S, Tone B, Tian H, Cole D, Pearce W. Core and penumbral nitric oxide synthase activity during cerebral ischemia and reperfusion. *Stroke*. 1998;29(5):1037–1046.
39 Zhang X, Xie Y, Wang H, et al. Symptomatic intracranial hemorrhage after mechanical thrombectomy in chinese ischemic stroke patients: the asian score. *Stroke*. 2020;51(9):2690–2696.
40 Ringelstein E, Droste D, Babikian V, et al. Consensus on microembolus detection by tcd. International consensus group on microembolus detection. *Stroke*. 1998;29(3):725–729.
41 Zhang X, Peng M, Feng C, et al. Nomogram predicting early neurological improvement in ischaemic stroke patients treated with endovascular thrombectomy. *Eur J Neurol*. 2021;28(1):152–160.
42 Durrleman S, Simon R. Flexible regression models with cubic splines. *Stat Med*. 1989;8(5):551–561.
43 Rothberg KG, Heuser JE, Donzell WC, Ying YS, Glenney JR, Anderson RG. Caveolin, a protein component of caveolae membrane coats. *Cell*. 1992;68(4):673–682.
44 Buitrago C, Boland R. Caveolae and caveolin-1 are implicated in 1alpha,25(oh)2-vitamin d3-dependent modulation of src, mapk cascades and vdr localization in skeletal muscle cells. *J Steroid Biochem Mol Biol*. 2010;121(1-2):169–175.
45 Hill MM, Bastiani M, Luetterforst R, et al. Ptrf-cavin, a conserved cytoplasmic protein required for caveola formation and function. *Cell*. 2008;132(1):113–124.
46 Kleinschnitz C, Pozgajova M, Pham M, Bendszus M, Nieswandt B, Stoll G. Targeting platelets in acute experimental stroke: Impact of glycoprotein ib, vi, and iib/iiia blockade on infarct size, functional outcome, and intracranial bleeding. *Circulation*. 2007;115(17):2323–2330.
47 Kraft P, Schuhmann MK, Fluri F, et al. Efficacy and safety of platelet glycoprotein receptor blockade in aged and comorbid mice with acute experimental stroke. *Stroke*. 2015;46(12):3502–3506.
48 Adams Jr. HP, Effron MB, Torner J, et al. Emergency administration of abciximab for treatment of patients with acute ischemic stroke: results of an international phase iii trial: Abciximab in emergency treatment of stroke trial (abestt-ii). *Stroke*. 2008;39(1):87–99.
49 Dhanesha N, Ahmad A, Prakash P, Doddapattar P, Lentz SR, Chauhan AK. Genetic ablation of extra domain a of fibronectin in hypercholesterolemic mice improves stroke outcome by reducing thrombo-inflammation. *Circulation*. 2015;132(23):2237–2247.
50 Dhanesha N, Chorawala MR, Jain M, et al. Fn-eda (fibronectin containing extra domain a) in the plasma, but not endothelial cells, exacerbates stroke outcome by promoting thrombo-inflammation. *Stroke*. 2019;50(5):1201–1209.
51 Göb E, Reymann S, Langhauser F, et al. Blocking of plasma kallikrein ameliorates stroke by reducing thromboinflammation. 2015;77(5): 784-803.
52 Chen C, Li T, Zhao Y, et al. Platelet glycoprotein receptor ib blockade ameliorates experimental cerebral ischemia-reperfusion injury by strengthening the blood-brain barrier function and anti-thrombo-inflammatory property. *Brain Behav Immun*. 2018;69:255–263.
53 Senchenkova EY, Ansari J, Becker F, et al. Novel role for the anx1-fpr2/alx signaling axis as a key regulator of platelet function to promote resolution of inflammation. *Circulation*. 2019;140(4):319–335.
54 Biswas I, Khan GA. Endothelial dysfunction in cardiovascular diseases. (eds). In: Shad KF, Luqman N, Saravi SSS, eds. *Basic and Clinical Understanding of Microcirculation*. London: IntechOpen; 2019.
55 Choudhary S, Sharma K, Singh PK. Von Willebrand factor: a key glycoprotein involved in thrombo-inflammatory complications of COVID-19. *Chem Biol Interact*. 2021;348:109657.
56 Busija AR, Patel HH, Insel PA. Caveolins and cavins in the trafficking, maturation, and degradation of caveolae: implications for cell physiology. *Am J Physiol Cell Physiol*. 2017;312(4):C459–C477.
57 Zhang Y, Chen K, Sloan SA, et al. An rna-sequencing transcriptome and splicing database of glia, neurons, and vascular cells of the cerebral cortex. *J Neurosci*. 2014;34(36):11929–11947.
58 Kaur H, Sarmah D, Saraf J, et al. Noncoding rnas in ischemic stroke: time to translate. *Ann N Y Acad Sci*. 2018;1421(1):19–36.
59 Yin K-J, Hamblin M, Chen YE. Non-coding rnas in cerebral endothelial pathophysiology: emerging roles in stroke. *Neurochem Int*. 2014;77:9–16.
60 Pan J, Qu M, Li Y, et al. Microrna-126-3p/-5p overexpression attenuates blood-brain barrier disruption in a mouse model of middle cerebral artery occlusion. *Stroke*. 2020;51(2):619–627.
61 Bernstein DL, Zuluaga-Ramirez V, Gajghate S, et al. Mir-98 reduces endothelial dysfunction by protecting blood–brain barrier (bbb) and improves neurological outcomes in mouse ischemia/reperfusion stroke model. *J Cereb Blood Flow Metab*. 2020;40(10):1953–1965.
62 Ren X, Jing Y-X, Zhou Z-W, Yang J-W. Knockdown of circrna-memo1 reduces hypoxia/reoxygenation injury in human brain endothelial cells through mirna-17-5p/sos1 axis. *Mol Neurobiol*. 2022;59(4):2085–2097.
63 Bai Y, Zhang Y, Han B, et al. Circular rna dlgap4 ameliorates ischemic stroke outcomes by targeting mir-143 to regulate endothelial-mesenchymal transition associated with blood–brain barrier integrity. *J Neurosci*. 2018;38(1):32–50.
64 Lee CY, Lai TY, Tsai MK, et al. The ubiquitin ligase ZNRF1 promotes caveolin-1 ubiquitination and degradation to modulate inflammation. *Nat Commun*. 2017;8:15502.
65 Jasmin J, Malhotra S, Singh Dhallu M, Mercier I, Rosenbaum D, Lisanti M. Caveolin-1 deficiency increases cerebral ischemic injury. *Circ Res*. 2007;100(5):721–729.
66 Blochet C, Buscemi L, Clément T, Gehri S, Badaut J, Hirt L. Involvement of caveolin-1 in neurovascular unit remodeling after stroke: effects on neovascularization and astrogliosis. *J Cereb Blood Flow Metab*. 2020;40(1):163–176.
67 Choi K, Kim H, Park M, et al. Regulation of caveolin-1 expression determines early brain edema after experimental focal cerebral ischemia. *Stroke*. 2016;47(5):1336–1343.
68 Knowland D, Arac A, Sekiguchi K, et al. Stepwise recruitment of transcellular and paracellular pathways underlies blood-brain barrier breakdown in stroke. *Neuron*. 2014;82(3):603–617.
69 Wang X, Kim H, Song R, Choi A. Caveolin-1 confers antiinflammatory effects in murine macrophages via the mkk3/p38 mapk pathway. *Am J Respir Cell Mol Biol*. 2006;34(4):434–442.
70 Jasmin J-F, Malhotra S, Singh Dhallu M, et al. Caveolin-1 deficiency increases cerebral ischemic injury. 2007; 100(5):721–729.
71 Xu S, Xue X, You K, Fu J. Caveolin-1 regulates the expression of tight junction proteins during hyperoxia-induced pulmonary epithelial barrier breakdown. *Respir Res*. 2016;17(1):50.

72 Bauer PM, Yu J, Chen Y, et al. Endothelial-specific expression of caveolin-1 impairs microvascular permeability and angiogenesis. *Proc Natl Acad Sci USA*. 2005;102(1):204–209.

73 Krezel W, Kastner P, Chambon P. Differential expression of retinoid receptors in the adult mouse central nervous system. *Neuroscience*. 1999;89(4):1291–1300.

74 Bookout AL, Jeong Y, Downes M, Yu RT, Evans RM, Mangelsdorf DJ. Anatomical profiling of nuclear receptor expression reveals a hierarchical transcriptional network. *Cell*. 2006;126(4):789–799.

75 Krzyzosiak A, Szyszka-Niagolov M, Wietrzych M, Gobaille S, Muramatsu S, Krezel W. Retinoid x receptor gamma control of affective behaviors involves dopaminergic signaling in mice. *Neuron*. 2010;66(6):908–920.

76 Huang JK, Jarjour AA, Nait Oumesmar B, et al. Retinoid x receptor gamma signaling accelerates cns remyelination. *Nat Neurosci*. 2011;14(1):45–53.

77 Sanz MJ, Albertos F, Otero E, Juez M, Morcillo EJ, Piqueras L. Retinoid x receptor agonists impair arterial mononuclear cell recruitment through peroxisome proliferator-activated receptor-gamma activation. *J Immunol*. 2012;189(1):411–424.

78 Dawson MI, Xia Z. The retinoid x receptors and their ligands. *Biochim Biophys Acta*. 2012;1821(1):21–56.

79 Golledge J, Mangan S, Clancy P. Effects of peroxisome proliferator-activated receptor ligands in modulating tissue factor and tissue factor pathway inhibitor in acutely symptomatic carotid atheromas. *Stroke*. 2007;38(5):1501–1508.

80 Plutzky J. The ppar-rxr transcriptional complex in the vasculature: Energy in the balance. *Circ Res*. 2011;108(8):1002–1016.

81 van Neerven S, Kampmann E, Mey J. Rar/rxr and ppar/rxr signaling in neurological and psychiatric diseases. *Progr Neurobiol*. 2008;85(4):433–451.